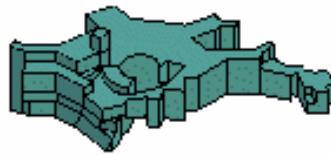


Cluster Halo Shapes and Substructure

Eric Hayashi

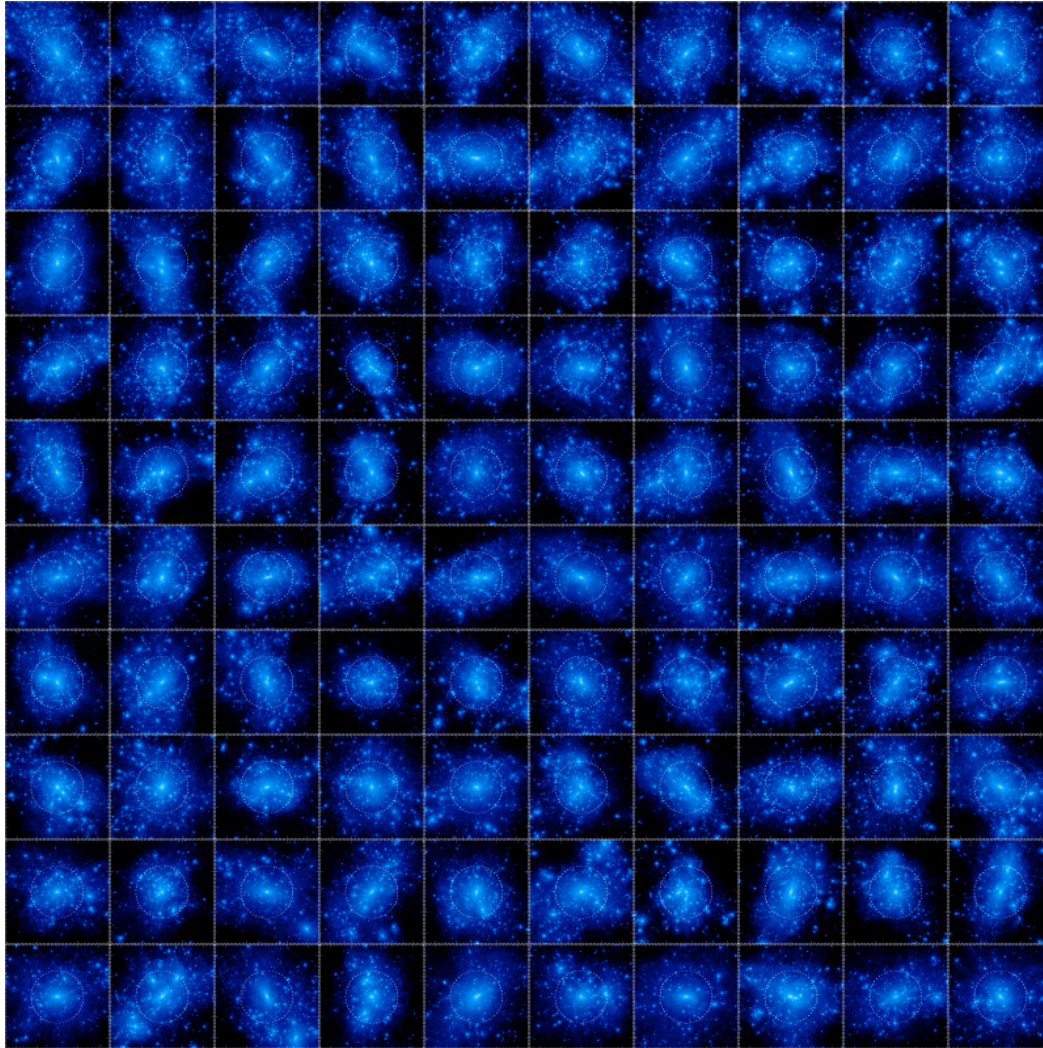
MPA Garching



MAX-PLANCK-GESELLSCHAFT

with Volker Springel, Simon White, Millennium Collaboration

Millennium Run Cluster Halos



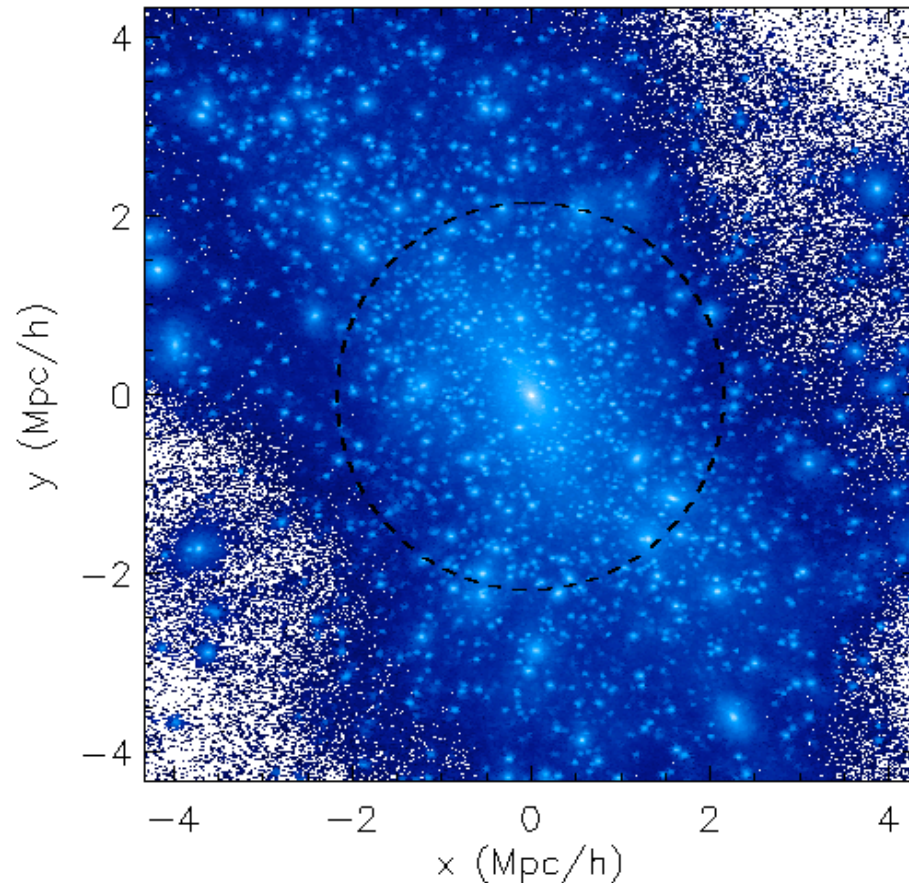
- 100 galaxy cluster-sized dark matter halos from Millennium Run simulation (Springel et al 2005)

- $3 \times 10^{14} < M_{200} < 3 \times 10^{15} M_{\odot}/h$
($m_{\text{part}} = 8.6 \times 10^8 M_{\odot}/h$)

- highly resolved structure and substructure

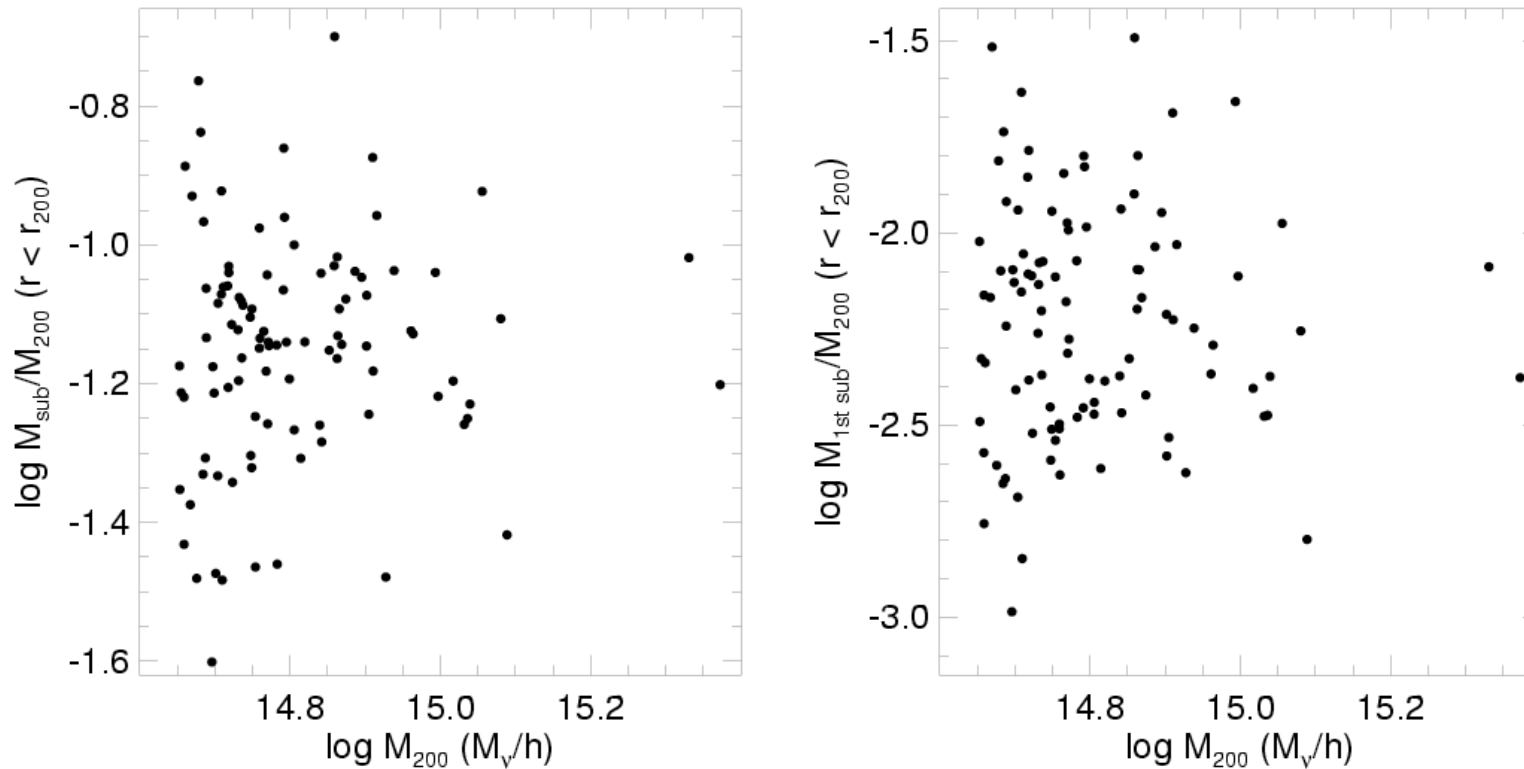
- unbiased sample of cluster halos in a large volume
($L_{\text{box}} = 500 \text{ Mpc}/h$)

Some Open Questions



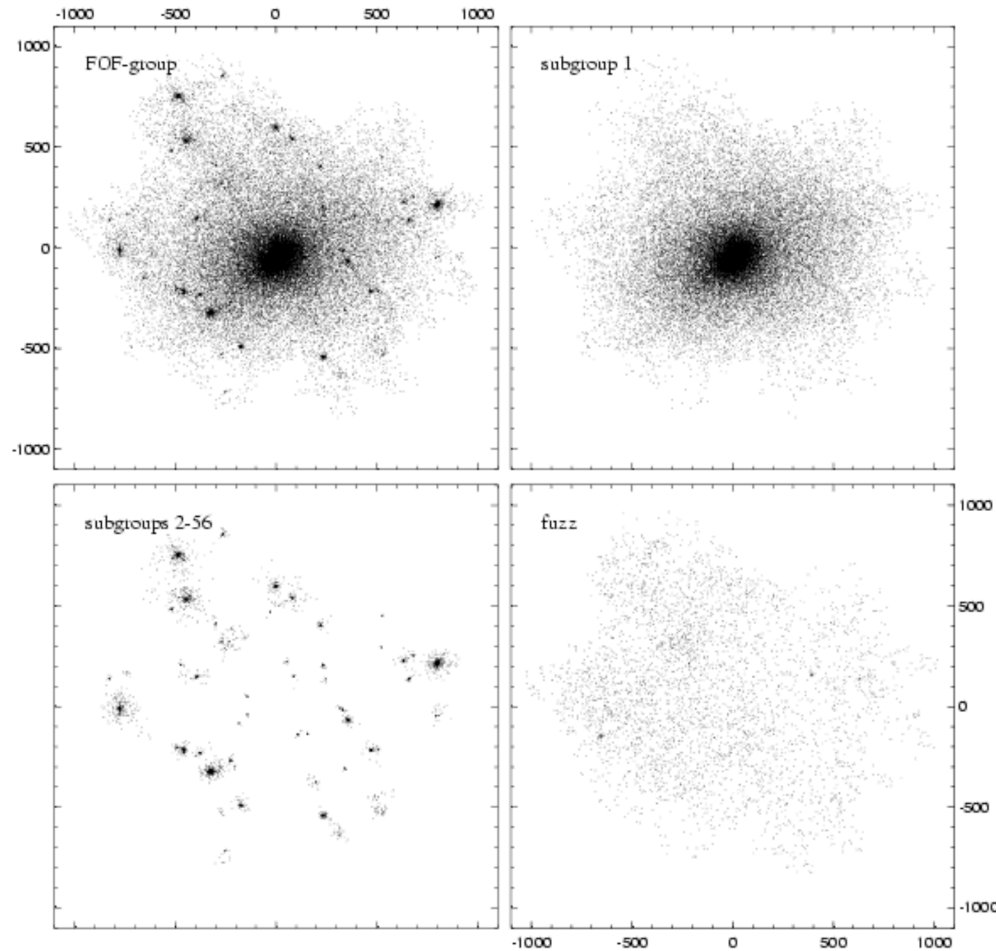
- 1) What is the spatial distribution of subhalos with respect to shape of host halos?
- 2) What is the distribution of shapes of subhalos compared to that of field halos?
- 3) How do the shapes of isodensity and isopotential surfaces of halos differ?
- 4) Is the distribution of projected shapes of halos consistent with gravitational lensing observations?

Cluster Halo Substructure Properties



- total mass in substructure within R_{200} ranges from 2% to 20% of M_{200} (avg $\sim 8\%$)
- most massive subhalo is at most 3% M_{200}

Substructure Identification



- substructures in Millennium run identified with SubFind (Springel et al 2001)
- identifies locally overdense, self-bound particles in subhalos and main background halo

Springel et al 2001

Characterizing Shape I

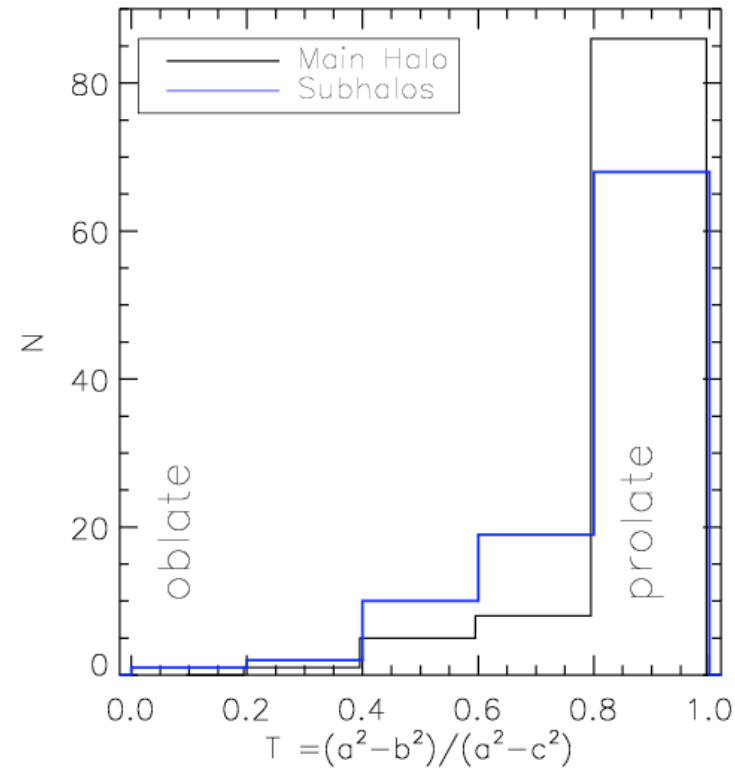
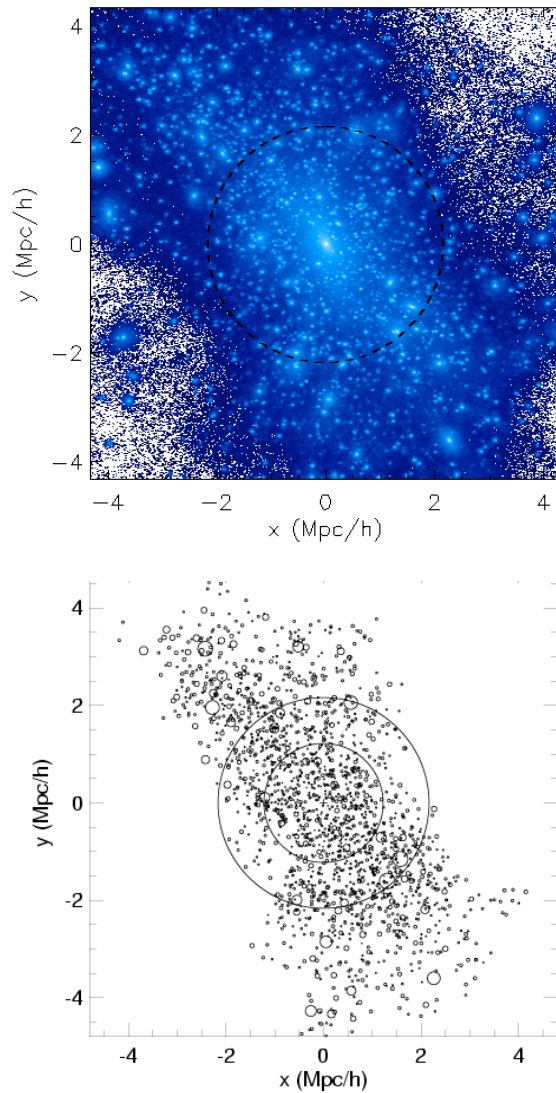
- calculate axis ratios of halo by diagonalizing inertia momentum tensor

$$M_{ij} = \Sigma x_i x_j / a^2$$

where $a = (x^2 + y^2/q^2 + z^2/s^2)^{1/2}$ and axial ratios $s \leq q \leq 1$

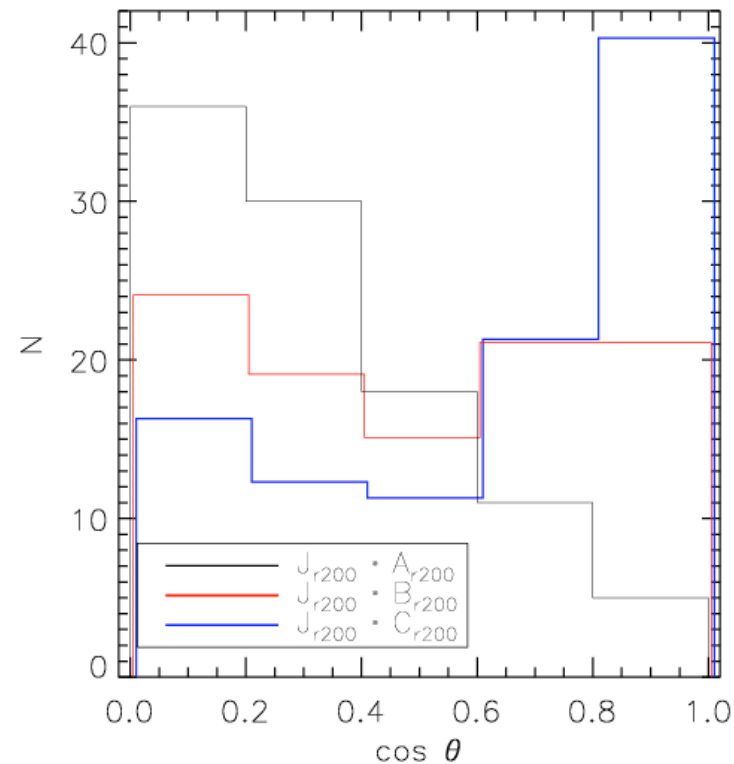
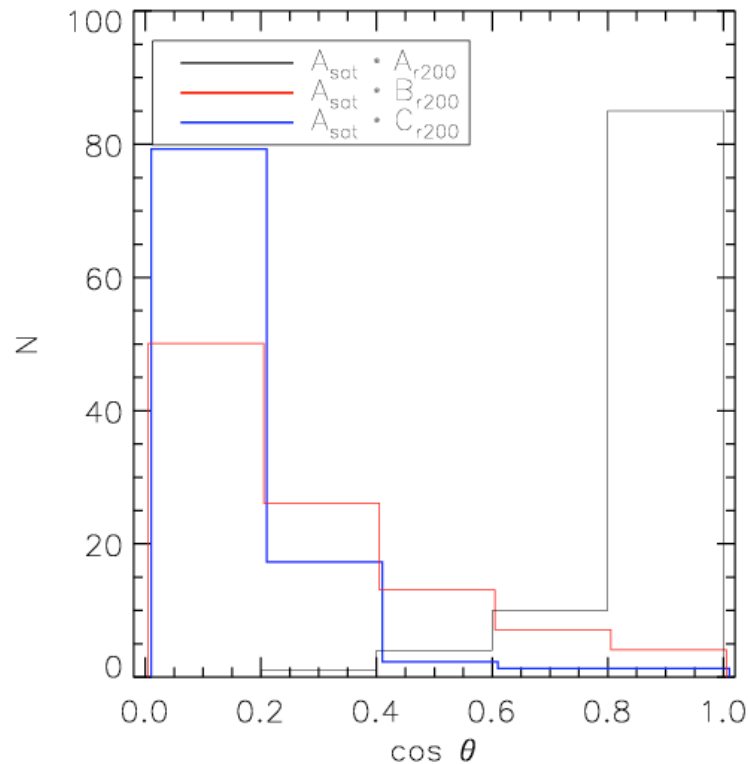
- determine unknown axial ratios by initially setting $s = q = 1$ and recalculating M_{ij} until axial ratio values converge (Katz 1991, Dubinski 1991)

Main Halo Shape and Subhalo Distribution



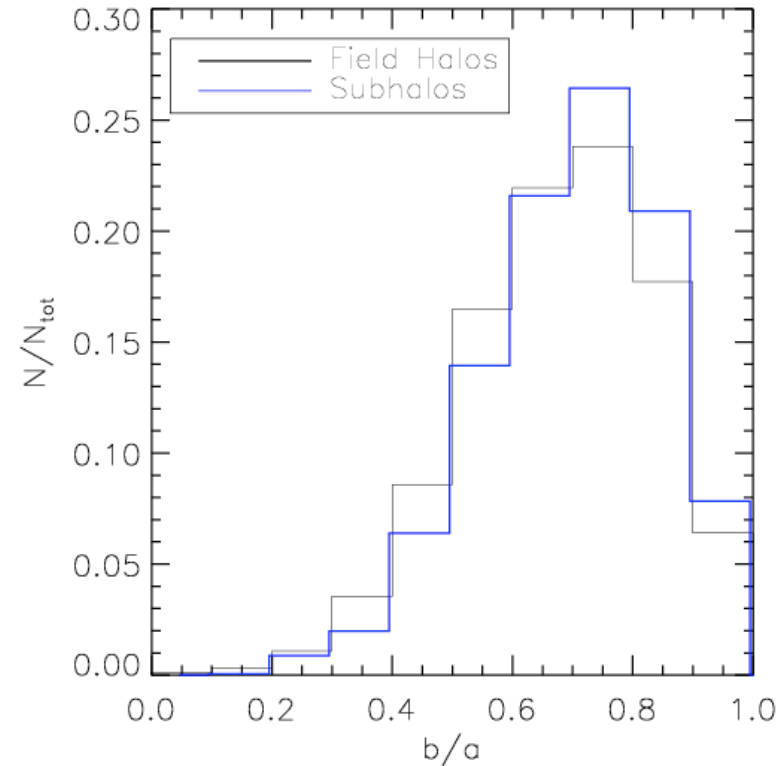
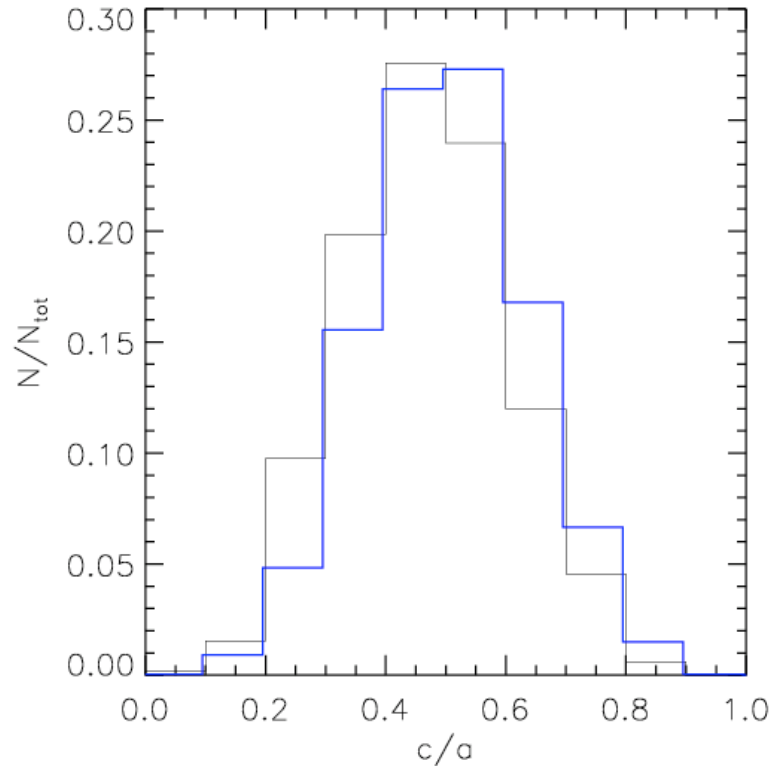
- prolate shapes strongly preferred by main halo and subhalo distribution

Millennium Run Cluster Halos



- major axis of satellite distribution is well-aligned with major axis of main halo and perpendicular to intermediate-minor axis plane
- angular momentum vector of halo is well-aligned with minor axis of halo in most cases, but can also be aligned with intermediate or minor axes

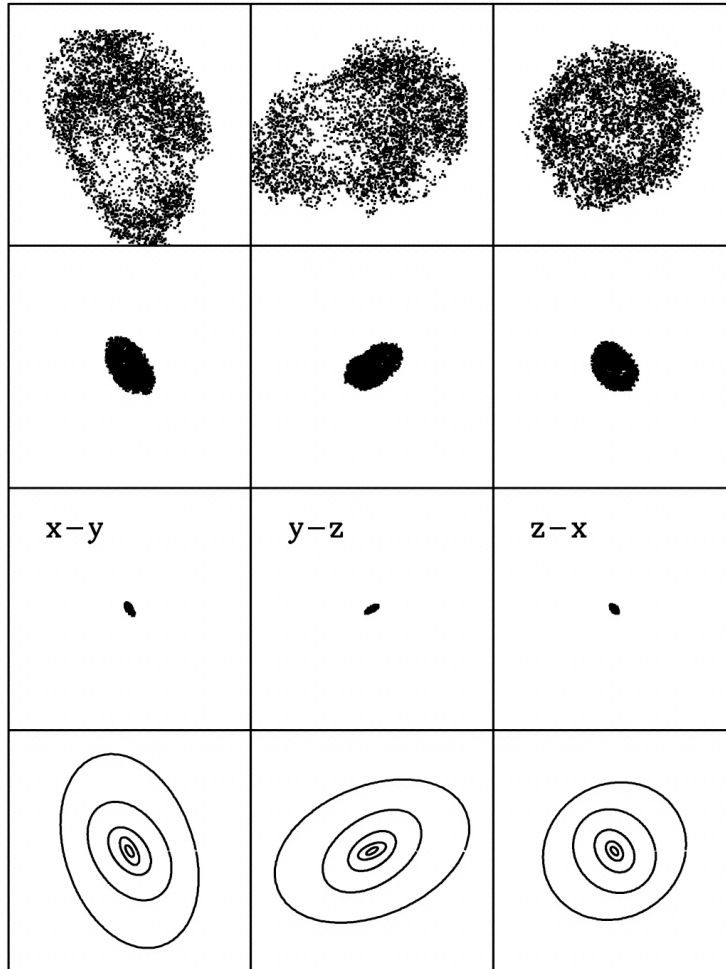
Shapes of Subhalos vs. Field Halos



- comparison of shapes for a sample of 3000 subhalos and equal number of field halos
- slight tendency toward rounder shapes for subhalos
- possibly the result of tidal heating by potential of cluster halo

Characterizing Shape II

CL3



- shapes of isodensity shells a la Jing & Suto 2001:

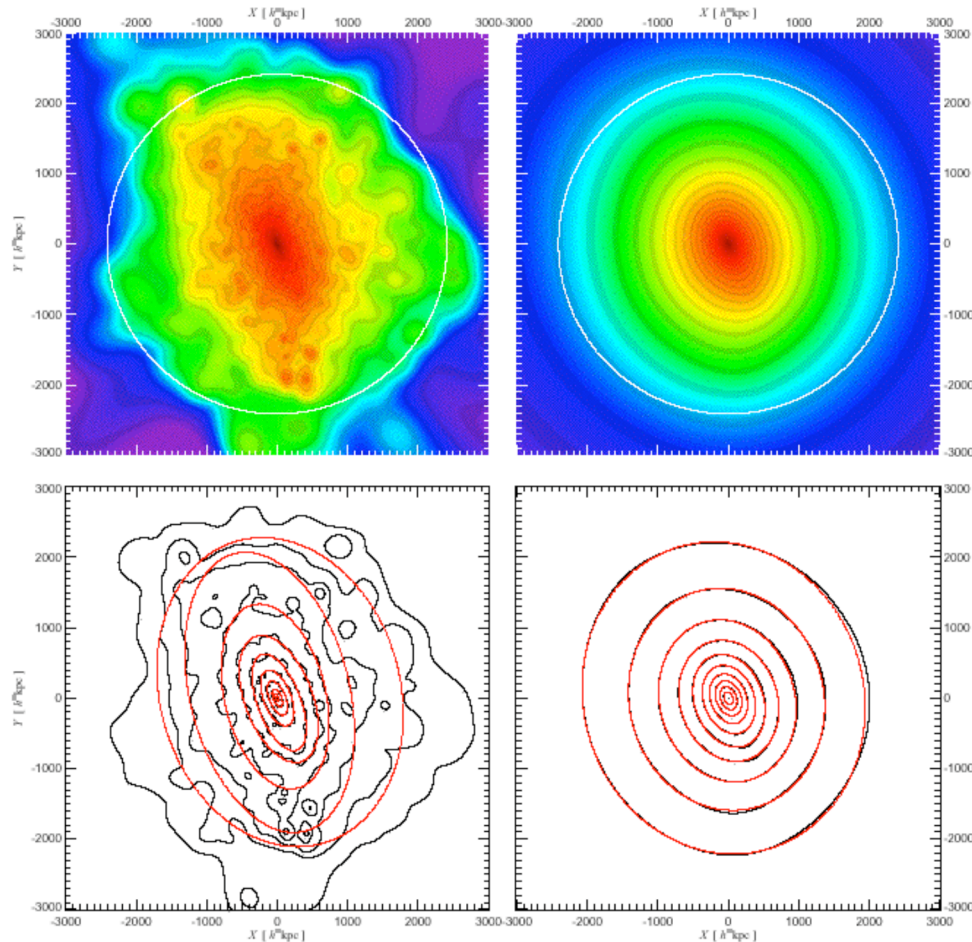
- remove substructure and isolate main halo

- compute local density of particles

- identify concentric shells of particles with equal local densities

- calculate inertia momentum tensor for particles in shells

Characterizing Shape II (cont'd)

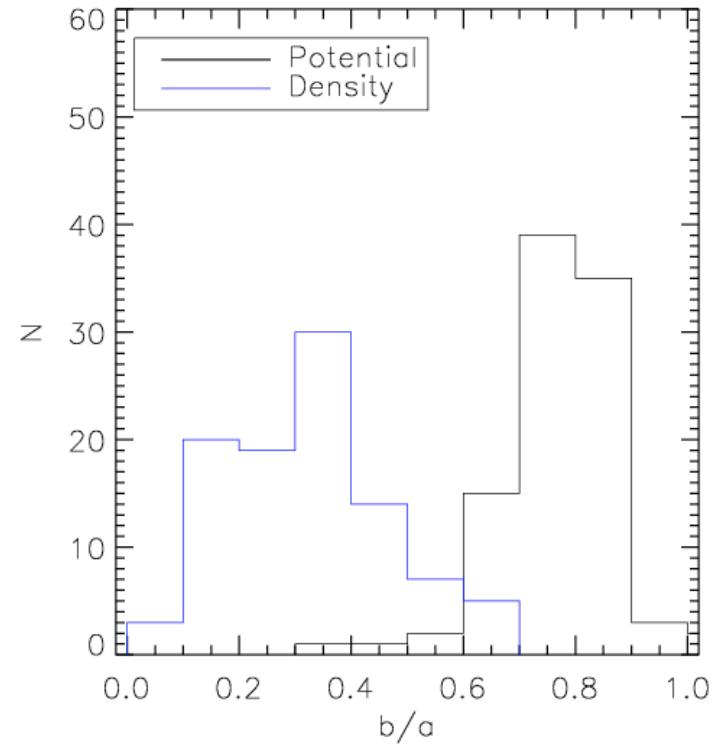
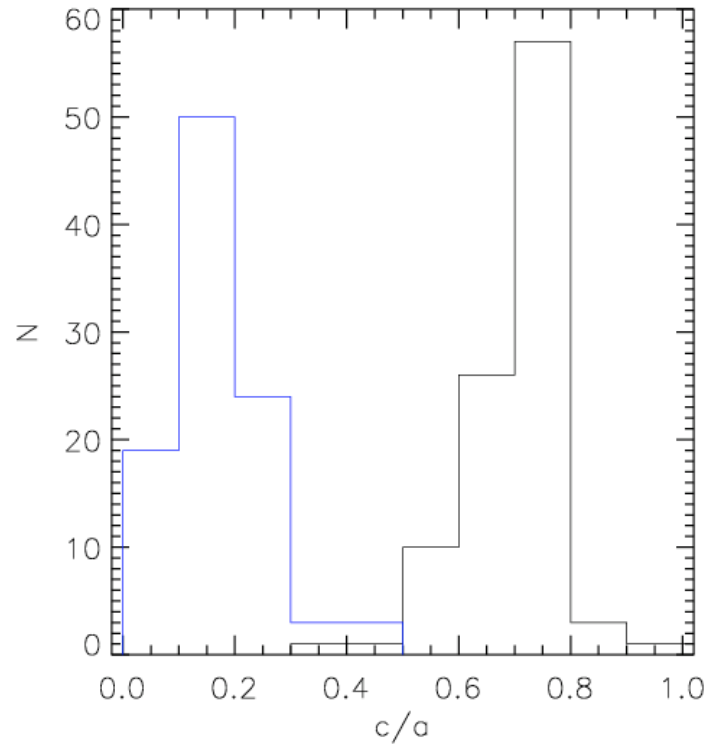


- shapes of isopotential surfaces a la Springel, White & Hernquist 2004:

➤ compute gravitational potential on 3 orthogonal planes through centre of halo

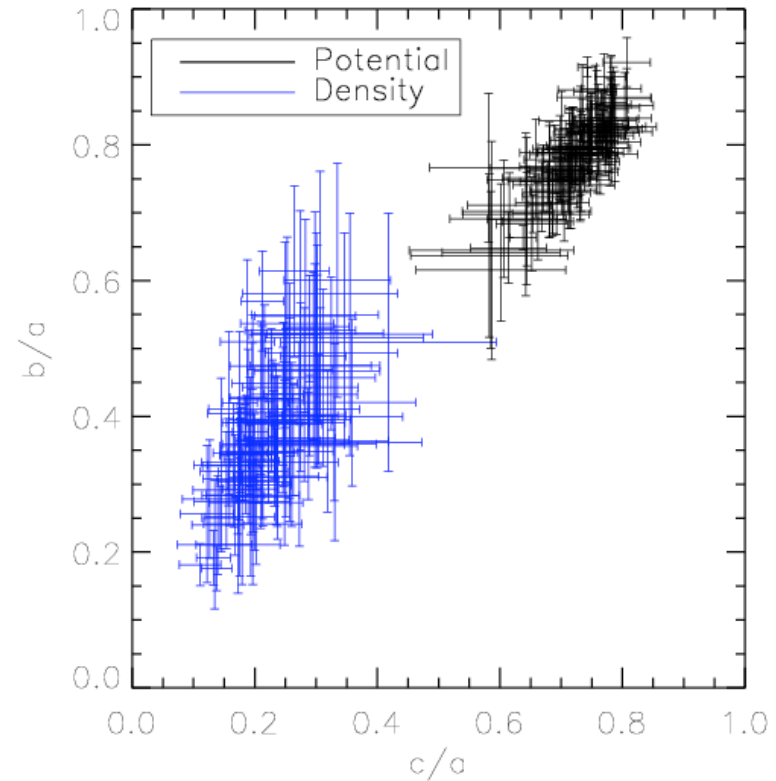
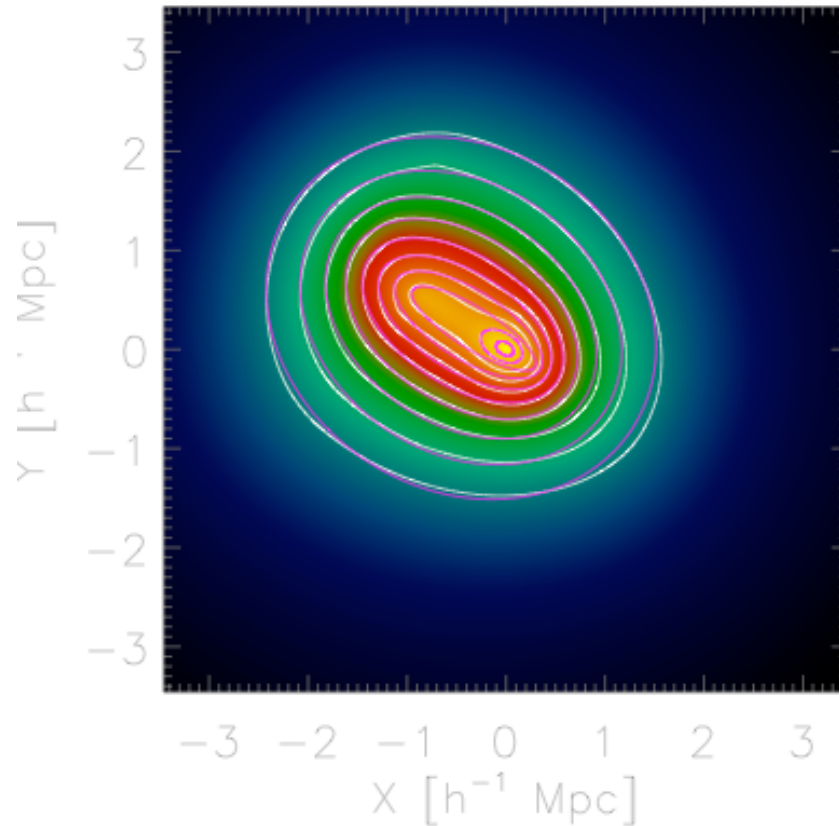
➤ fit 3D ellipsoid to isopotential contours on the planes

Comparison of Shape Measurements



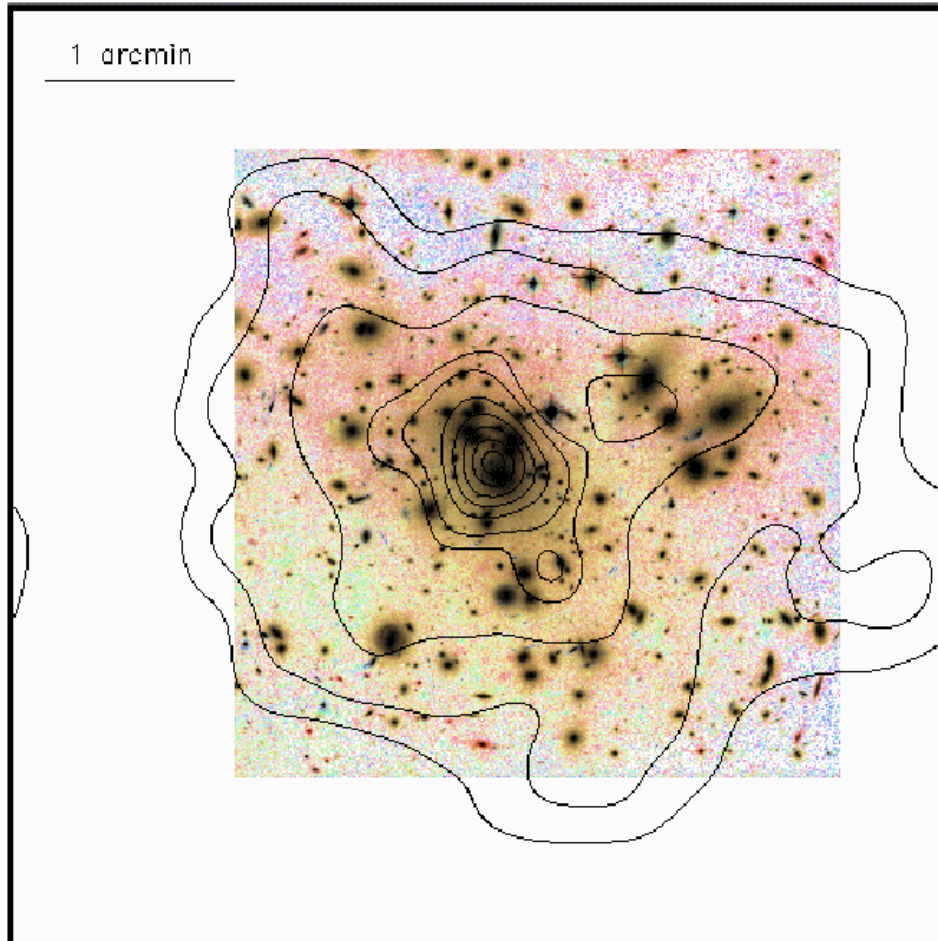
- both methods give shape as a function of radius so compare shapes at some fiducial radius (e.g. scale radius r_s from NFW fits to density profile)
- isopotential surfaces are significantly more spherical than isodensity shells (Springel, White & Hernquist 2004)

Comparison of Shape Measurements



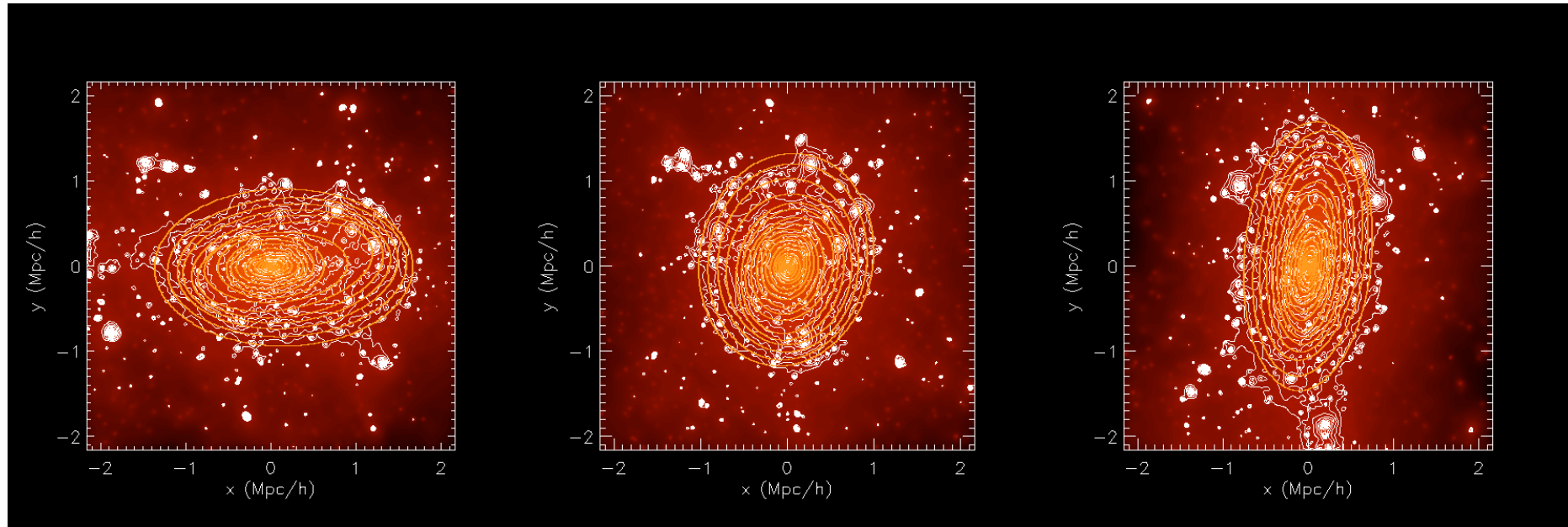
- shapes of isopotential surfaces are more stable with radius (halos are more spherical at large radii)
- some contours are not well fit by ellipses due to subhalos

Comparison with Lensing Observations



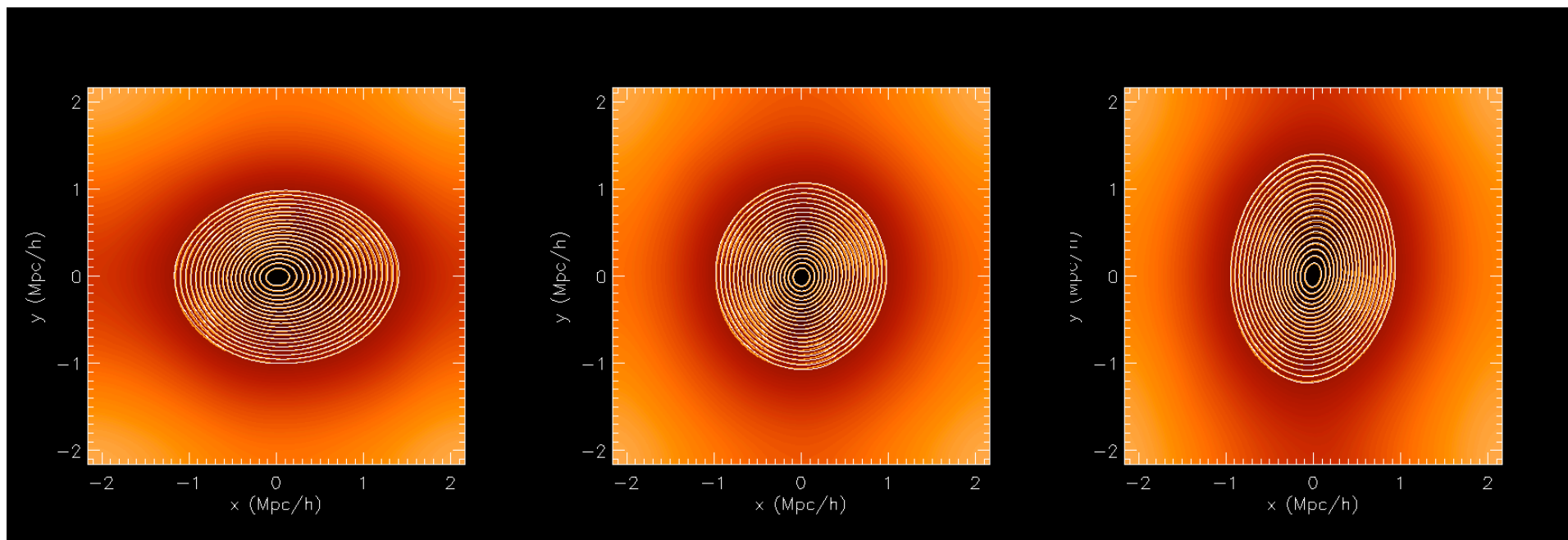
- compare simulated cluster halo shapes with reconstructed mass models of clusters from lensing observations
- e.g. nonparametric mass model of Abell 1689 of Diego, Sandvik et al (2005)
- are shapes of isodensity contours consistent with simulated halos?

Projected Density of Cluster Halos



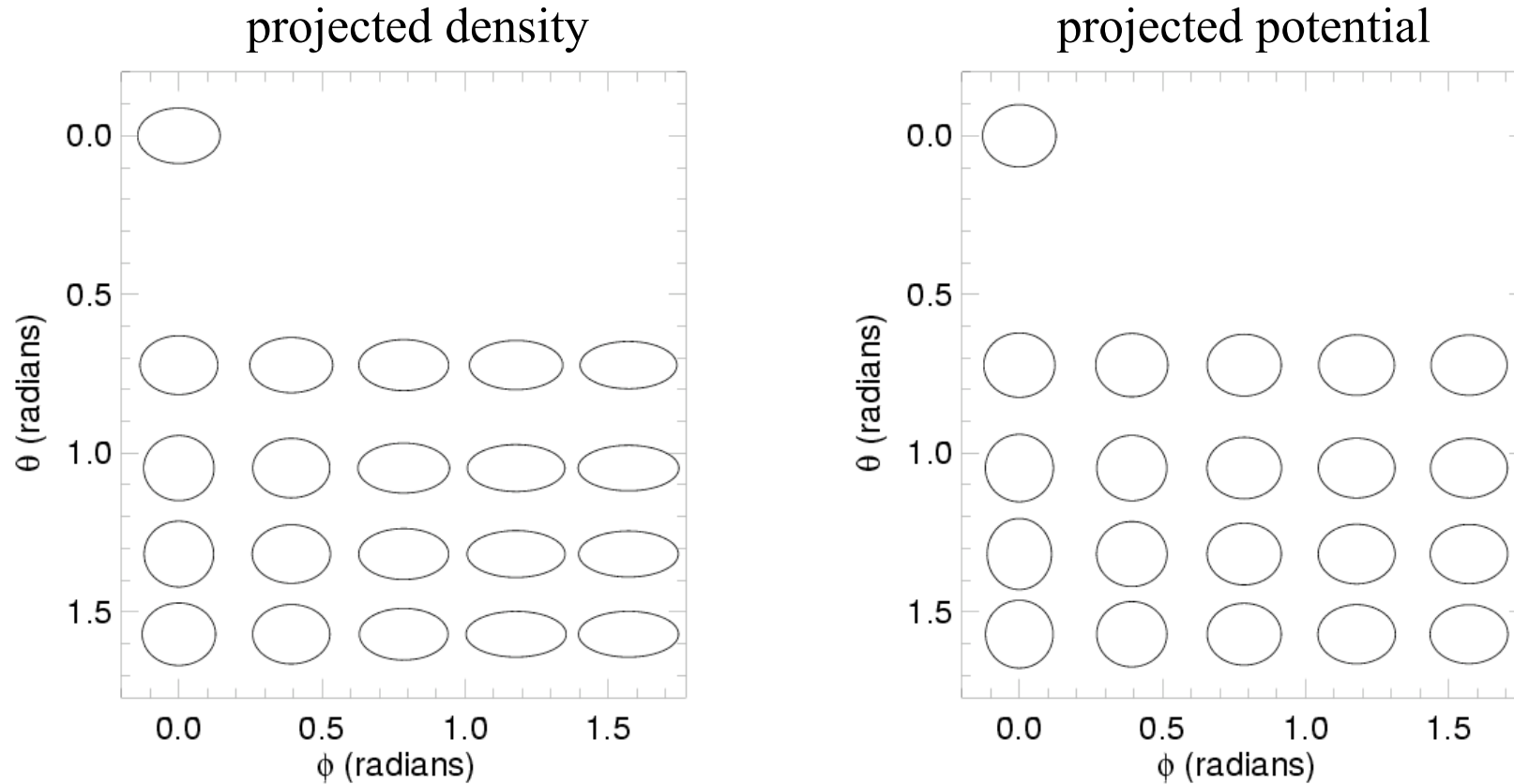
- compare halo shapes with projected mass models from gravitational lensing observations
- project density of cluster halos along different lines of sight and fit isodensity contours with ellipses
- contours often poorly approximated by ellipses due to substructure
- compare statistics of peaks in surface density instead?

Projected Potential of Cluster Halos



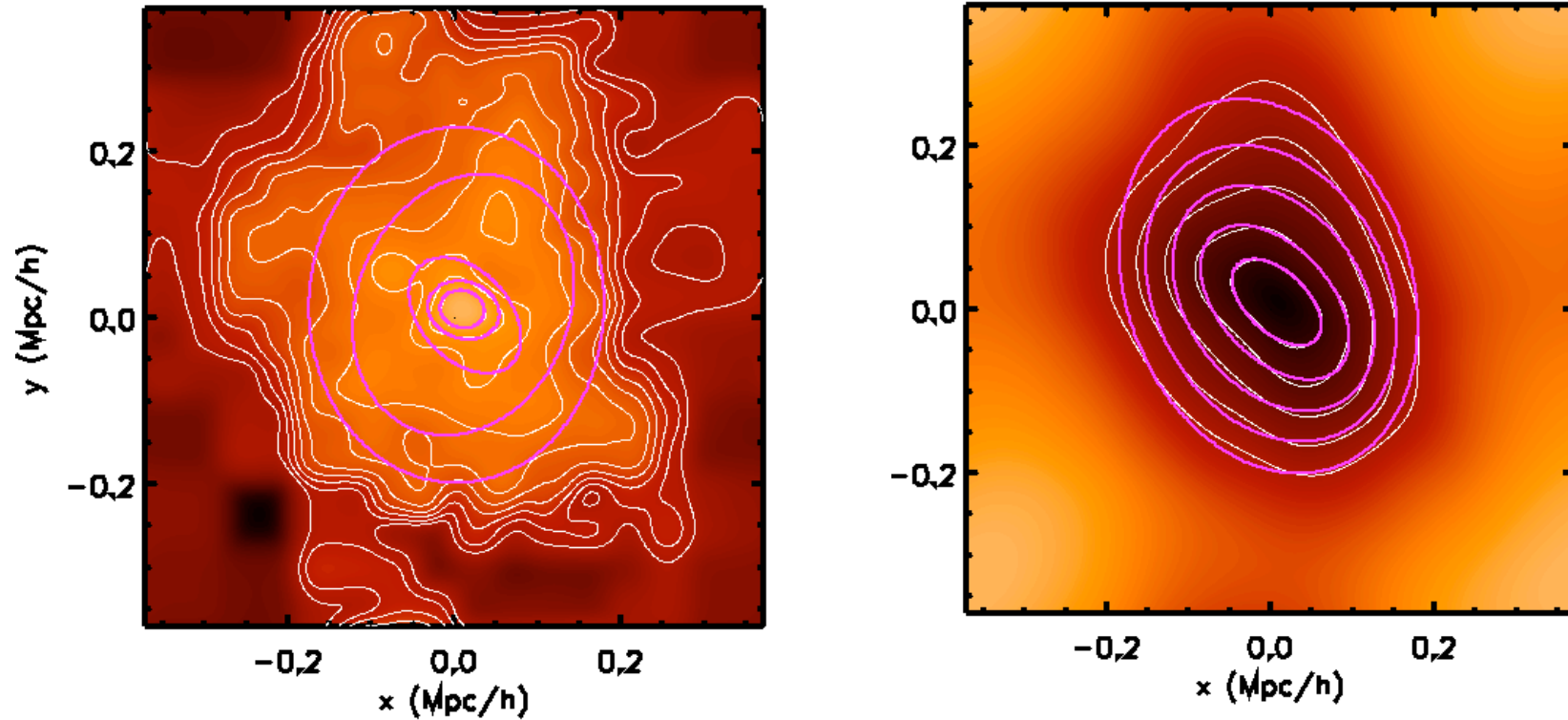
- shapes of projected potential much better approximated by ellipses
- ellipticity of contours is well-defined as function of radius

Projection Effects



- quantify scatter in ellipticity with viewing angle
- to do: use full halo sample to calculate expected distribution of ellipticities

Comparison with A1689



- will need large homogeneous sample of lensing clusters to compare with distribution of projected shapes predicted by simulations

Future Work

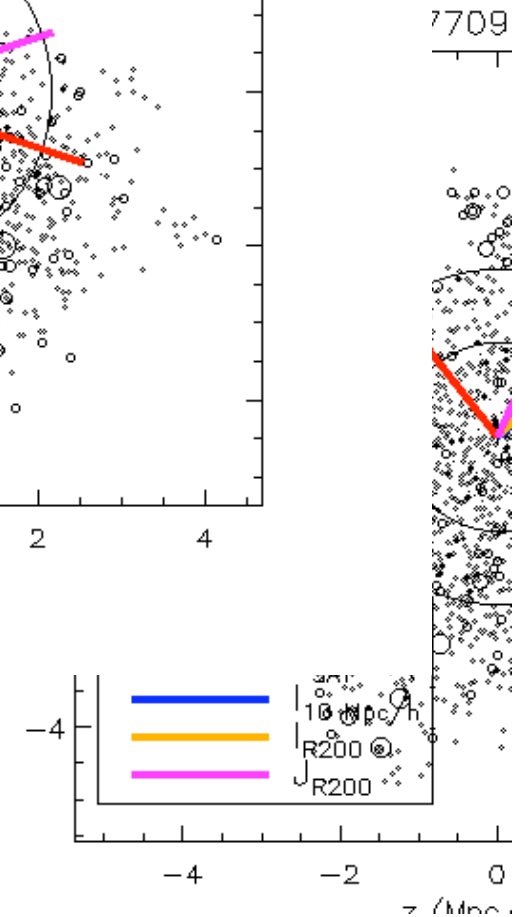
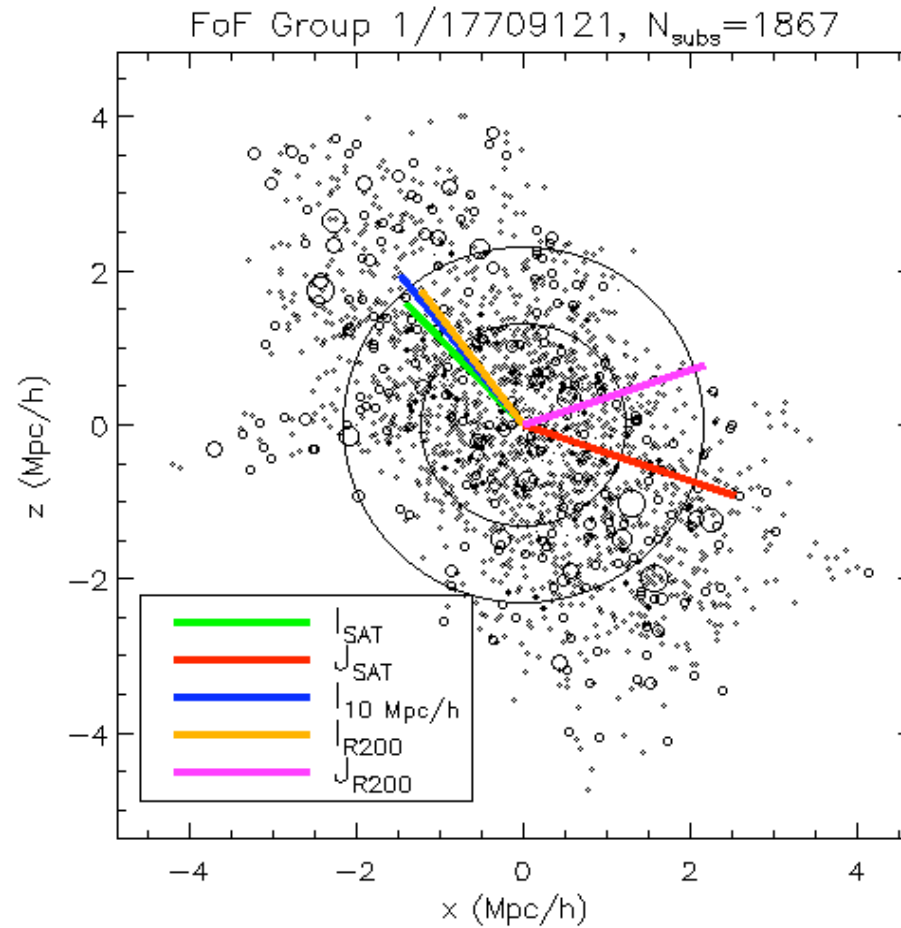
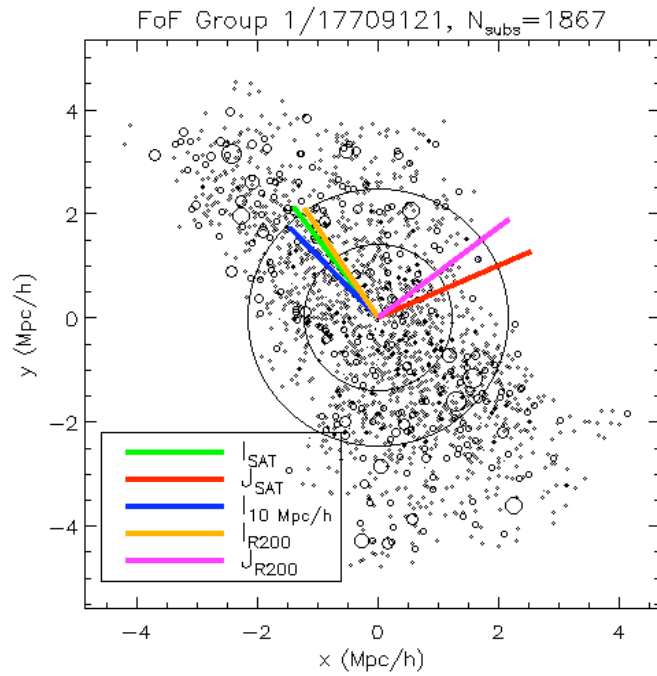
- Investigate origin of halo shapes and evolution with redshift
- Investigate correlations between shape and large scale structure, orientation of halos with respect to filamentary structure
- Comparison with analytic model for distribution of triaxialities of Lee, Jing & Suto 2005
- Quantify correlations between projected satellite galaxy distribution and projected density/potential contours

The End

June 2 2005

Trieste Conference

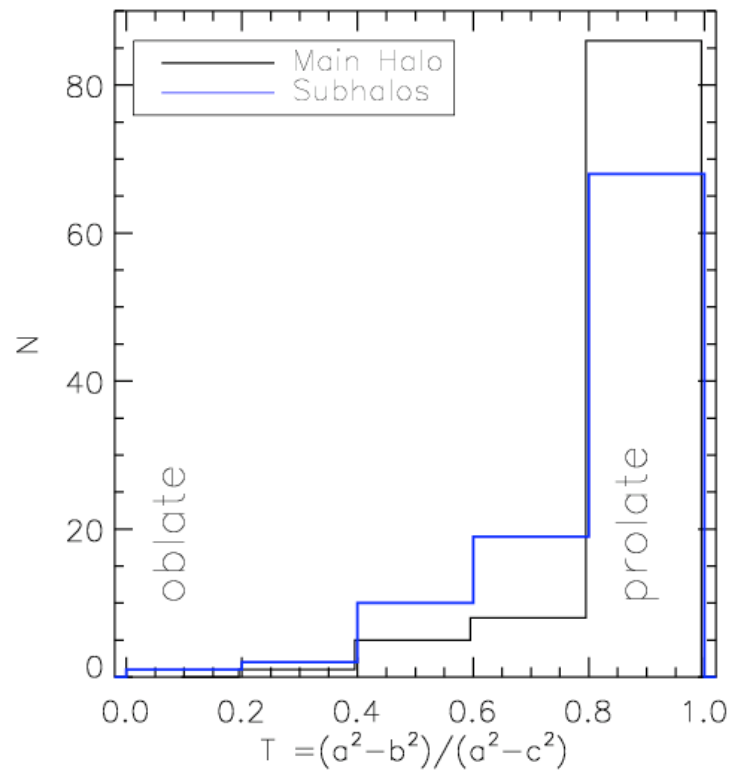
Millennium



June 2 2005

Trieste Conference

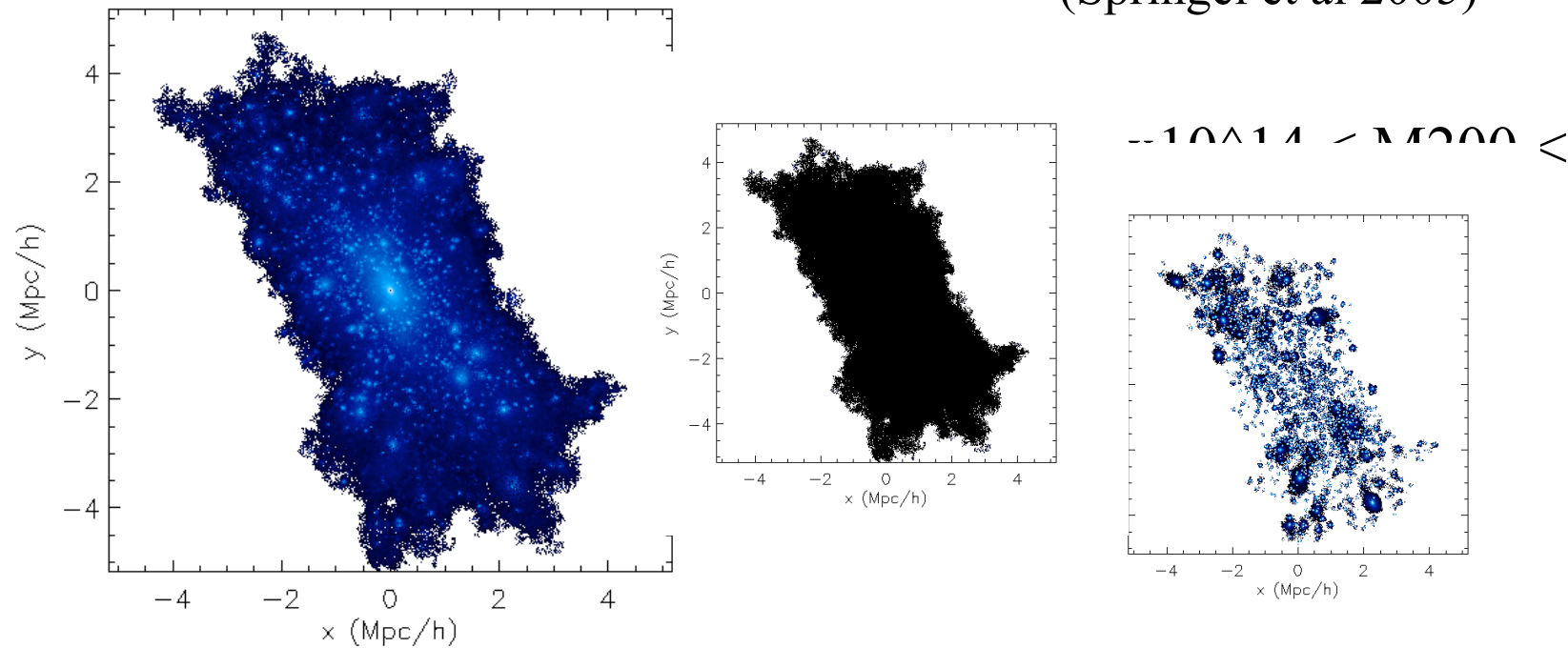
Millennium Run Cluster Halos



- 100 galaxy cluster-sized dark matter halos from Millennium Run simulation (Springel et al 2005)

Millennium Run Cluster Halos

- 100 galaxy cluster-sized dark matter halos from Millennium Run simulation (Springel et al 2005)



Giant Arc Statistics in the New Millennium

Eric Hayashi
ESO Lensing Seminar



June 2 2005

Trieste Conference

Testing CDM with Strong Lensing

- Two approaches:
 - 1) Using strongly lensed images to reconstruct the mass profile of individual clusters,

i.e., Can CDM halos reproduce observed pattern of arcs in a given cluster?
 - 2) Using cluster surveys to estimate the total number of observed strongly lensed images,

i.e., Does CDM predict the correct number of strongly lensed images?

Giant Arc Statistics

- Problem first noticed by various authors in early 1990's (Kochanek 1990, Hammer 1991, Miralda-Escude 1991):
 - Observed number of giant arcs may exceed number expected in CDM
- Investigated by Bartelmann in a series of papers
- Bartelmann & Weiss (1994) present initial method for calculating giant arcs produced by CDM galaxy cluster halo taken from cosmological N-body simulation
- For each simulated cluster halo, three surface density fields generated by projecting halo onto planes perpendicular to the principal axes of the inertial tensor of the halo

Giant Arc Statistics

- Deflection angle $\alpha(\mathbf{x})$ calculated on a regular grid on each lens plane
- Corresponding position on source plane defined by $\mathbf{y} = \mathbf{x} - \alpha(\mathbf{x})$
- Image points defined as all image-plane positions \mathbf{x} which map to source plane positions \mathbf{y} within a source radius r_s of source centre \mathbf{y}_c
- Contiguous sets of image points define strongly lensed images (arcs)
- Dimensions of arc determined by fitting ellipses to image points (giant arcs defined by $l/w \geq 10$)

Giant Arc Statistics

- Bartelmann et al (1998) perform calculation for numerous cluster halos from simulations of three different cosmologies
- *Conclude that the expected number of giant arcs in LCDM is an order of magnitude less than the number of observed arcs on the whole sky based on the EMSS cluster survey*
- Meneghetti, Bartelmann et al (2000) investigate the effect of cluster galaxies on arc statistics
- Cluster galaxies added “by hand” since their simulated halos had insufficient resolution to resolve substructure
- Use observed luminosity function to constrain distribution of galaxies, and assume light traces mass for spatial distribution

Giant Arc Statistics

- Find that cluster galaxies increase the length and curvature of critical curves

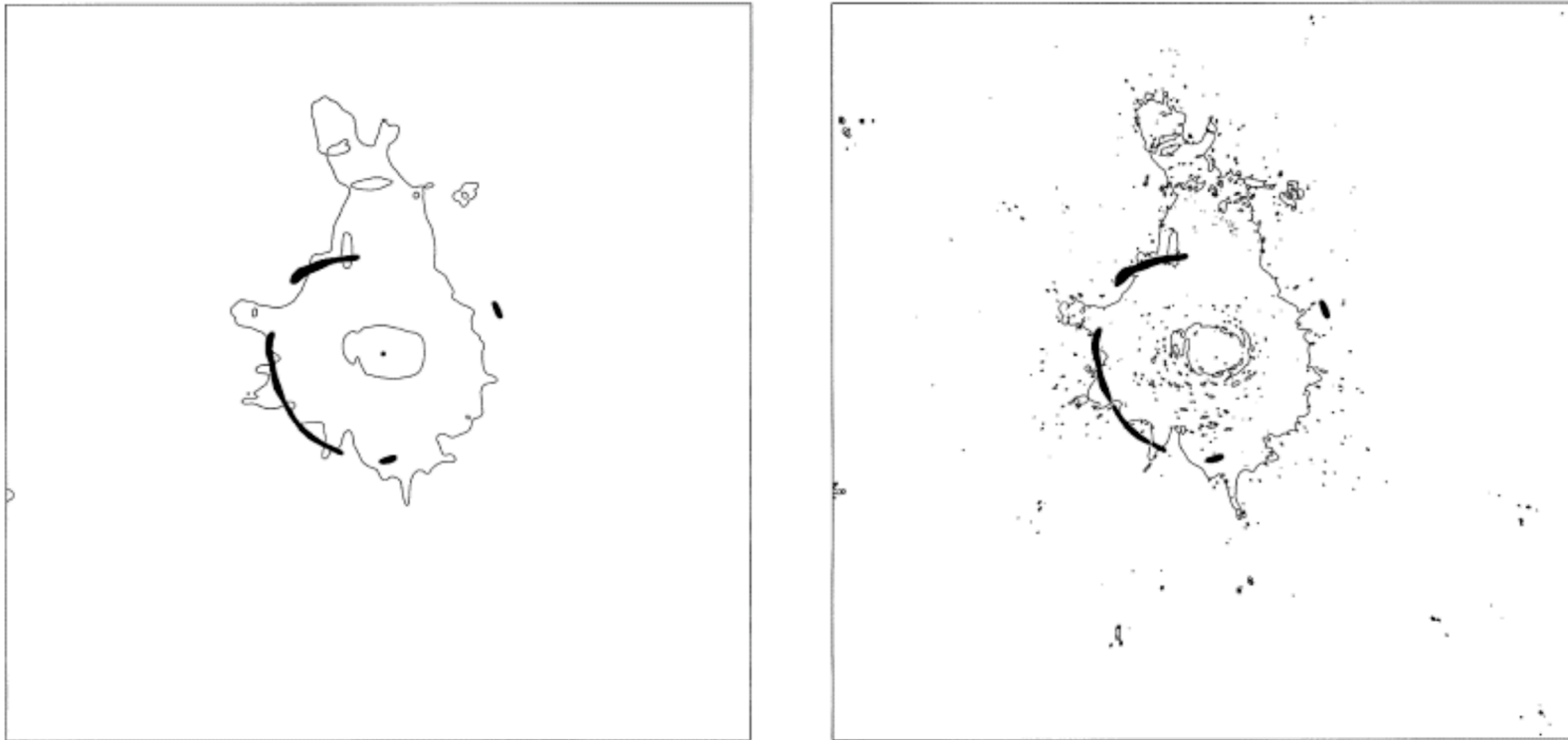


Figure 6. Example of critical curves and arcs obtained in a DM (left panel) and GAL simulations (right panel). The angular dimensions of the plot correspond to ≈ 333 arcsec. It can be noticed that the presence of galaxies acting as gravitational lenses can split long arcs in several arclets, and increases the length of the critical curves.

Giant Arc Statistics

- Conclude that cluster galaxies have overall an insignificant effect on arc statistics

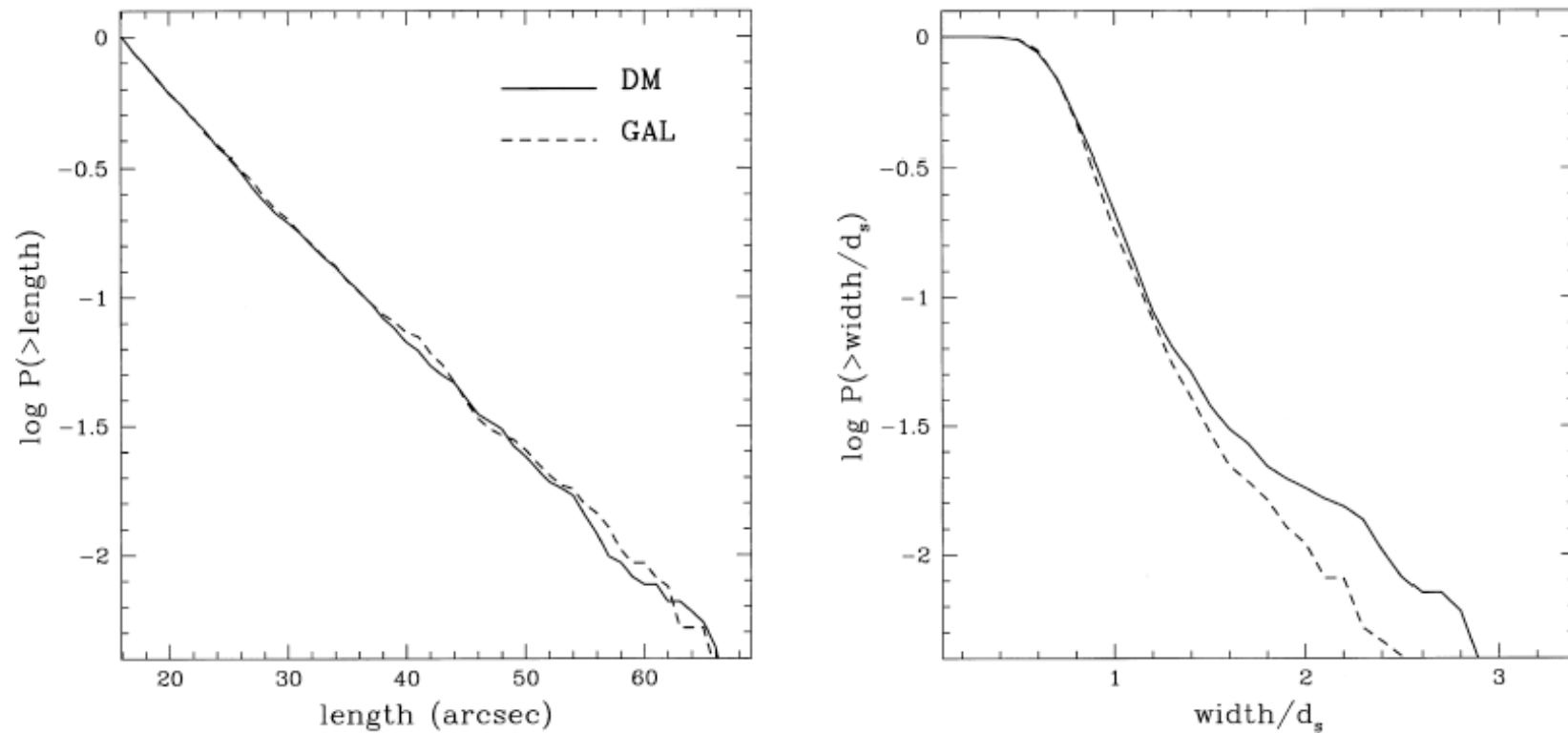


Figure 4. The cumulative distributions for the lengths l (in units of arcsec) and the widths w (in units of the source equivalent diameter $d_s = 2$ arcsec) are presented in the left and right panels, respectively. Results for the DM and GAL simulations are shown by solid and dashed lines, respectively. Typical bootstrap errors of the curves shown here grow from ~ 5 per cent for small arcs to ~ 15 per cent for large arcs.

Giant Arc Statistics

- Meneghetti, Bartelmann et al (2003) investigate the effect of a central cD galaxy on strong lensing properties of a galaxy cluster
- cD galaxies with masses between 5×10^{12} Msol/h and 5×10^{13} Msol/h added to simulated clusters with masses between 3×10^{14} Msol/h and 10^{15} Msol/h
- Find relative enhancements of large-arc cross-sections of up to a factor of two, but only by 50% in realistic cases
- Conclude that the presence of a cD galaxy is unable to account for the discrepancy between predicted and observed numbers of giant arcs

Giant Arc Statistics

- Dalal, Holder & Hennawi (2004) repeat calculation using methods similar to Bartelmann et al but find no discrepancy between predicted and observed number of giant arcs!
- Three factors of two combine to resolve the discrepancy:
 - 1) Use an estimate of source number density as a function of redshift based on Hubble Deep Field (vs. $z_s=1$ assumed by Bartelmann et al)
 - 2) Use an updated EMSS sample (38 clusters vs. 16 used in Bartelmann estimate)
 - 3) Find a higher lensing cross section for their simulated clusters than Bartelmann et al (not well understood)

Giant Arc Statistics

- Wambsganss, Bode & Ostriker (2004) also conclude that no discrepancy exists between observations and LCDM predictions
- Use multiplane lens equation instead of thin lens approximation
- But use magnification as a proxy for length-to-width ratio (i.e., assume $l/w = \mu$)
- Find that probability of highly magnified images increases significantly for as redshift of source plane is increased

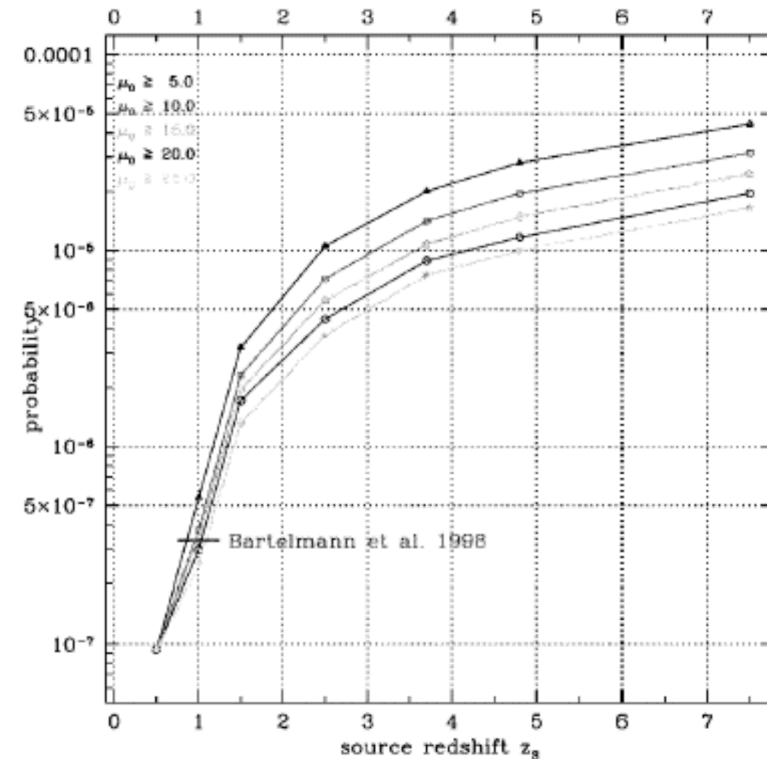


FIG. 1.—Probability for the occurrence of gravitationally lensed arcs with length-to-width ratios r (\approx magnifications μ_i) of ≥ 5 (triangles), ≥ 10 (squares), ≥ 15 (pentagons), ≥ 20 (circles), and ≥ 25 (stars) as a function of galaxy redshift z_s , for the LCDM model. For comparison, the probability as determined by B98 is indicated as a horizontal bar; they had assumed that all galaxies are at $z_s = 1$ and evaluated arcs with $r \geq 10$. [See the electronic edition of the *Journal* for a color version of this figure.]

Giant Arc Statistics

- Oguri et al (2004) use semi-analytic methods to predict arc statistics for LCDM
- Conclude that triaxiality *and* a steep halo cusp ($r^{-1.5}$) required to reconcile theoretical predictions with observations
- Latest N-body simulations do not support such a steep halo cusp (Hayashi et al 2004, Navarro et al 2004)

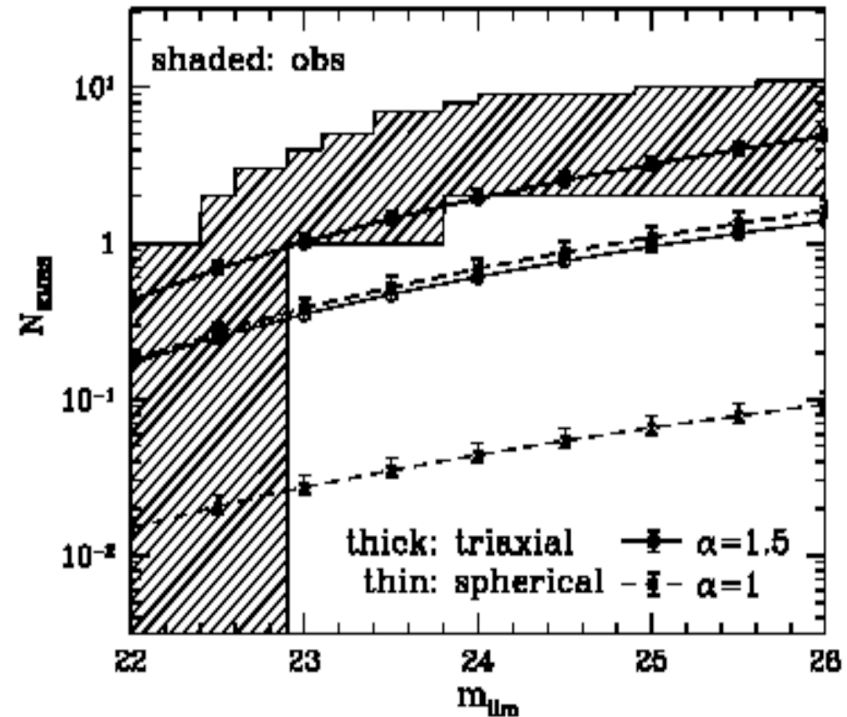
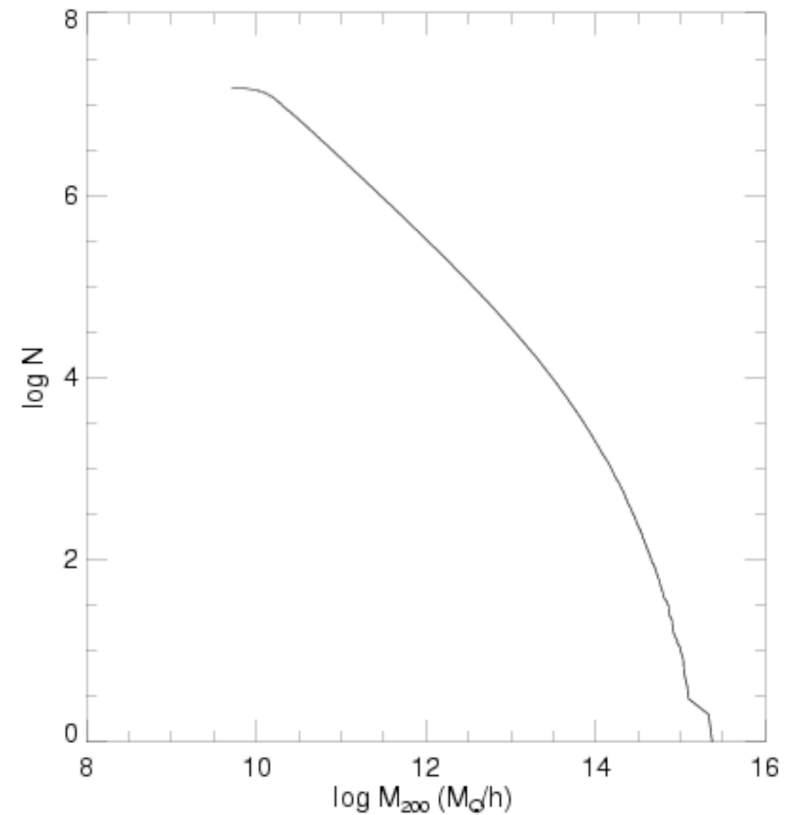
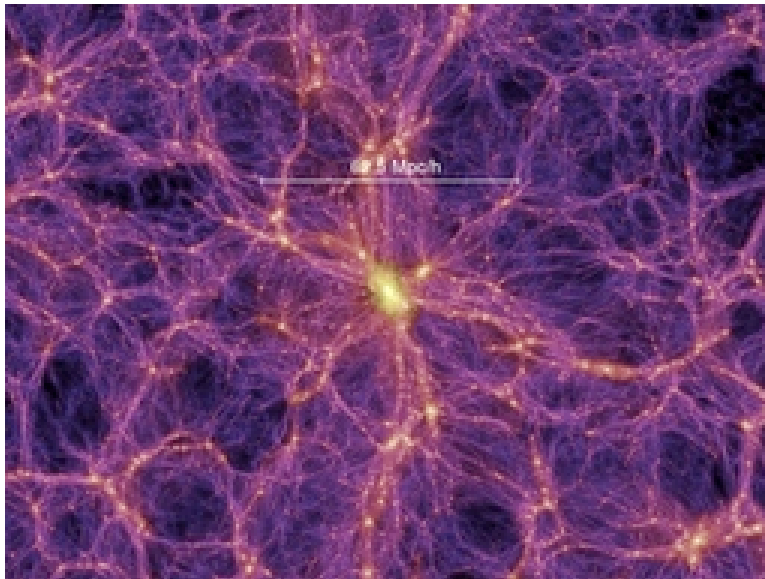


FIG. 12.—Number of arcs in the 38 EMSS cluster sample (eq. [64]) as a function of B -band limiting magnitude m_{lim} . The threshold axis ratio is $\epsilon_{\text{th}} = 10$. The observed number of arcs taking account of several uncertainties, which is shown by the shaded region, is discussed in § 5.2. [See the electronic edition of the Journal for a color version of this figure.]

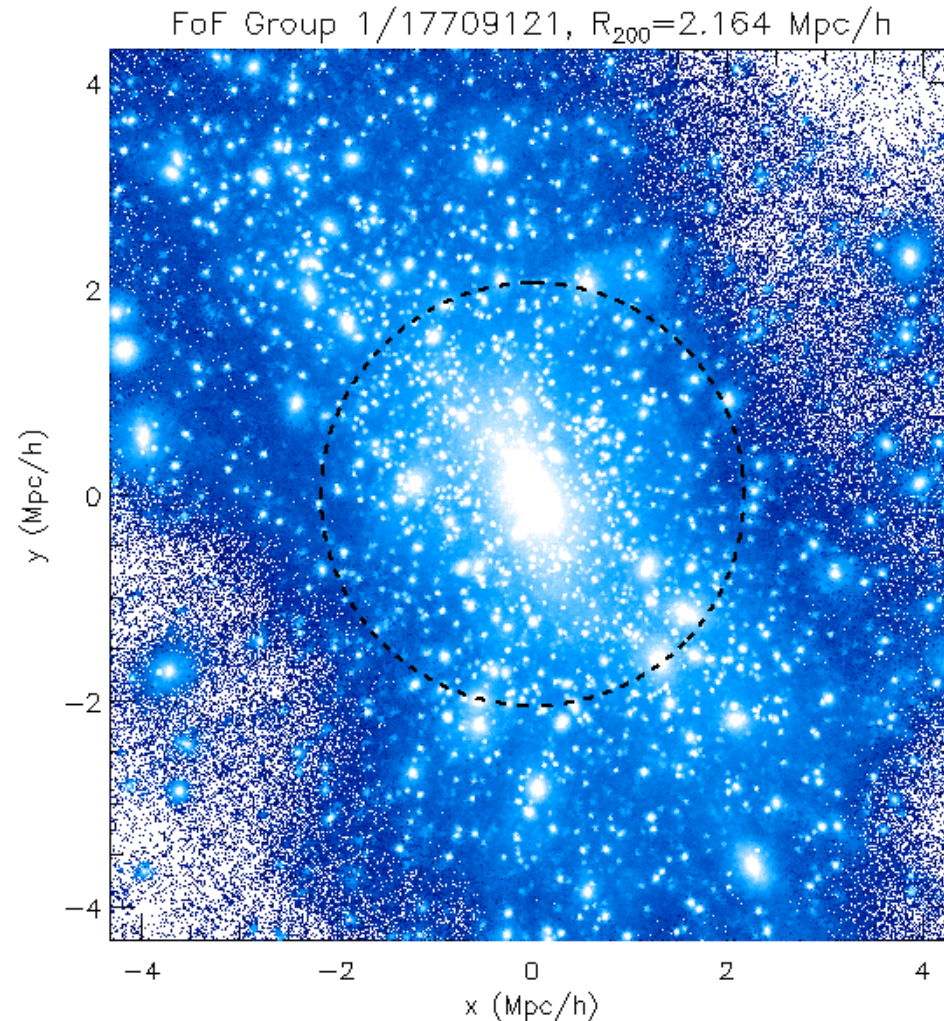
Giant Arc Statistics

- Millennium Run cosmological N-body simulation
- $N=10^{10}$
- $L_{\text{box}}=500 \text{ Mpc}/h$
- $m_{\text{part}} = 8 \times 10^8 \text{ Msol}/h$



Giant Arc Statistics

- Simulation contains large sample of massive clusters, ideal for investigating strong lensing properties as function of halo shape, concentration, substructure, etc.
- Can graft galaxies onto dark matter halos using semi-analytic codes to model baryonic component and investigate source distribution



The End

June 2 2005

Trieste Conference

Reconstructed Mass Map of CL 0024

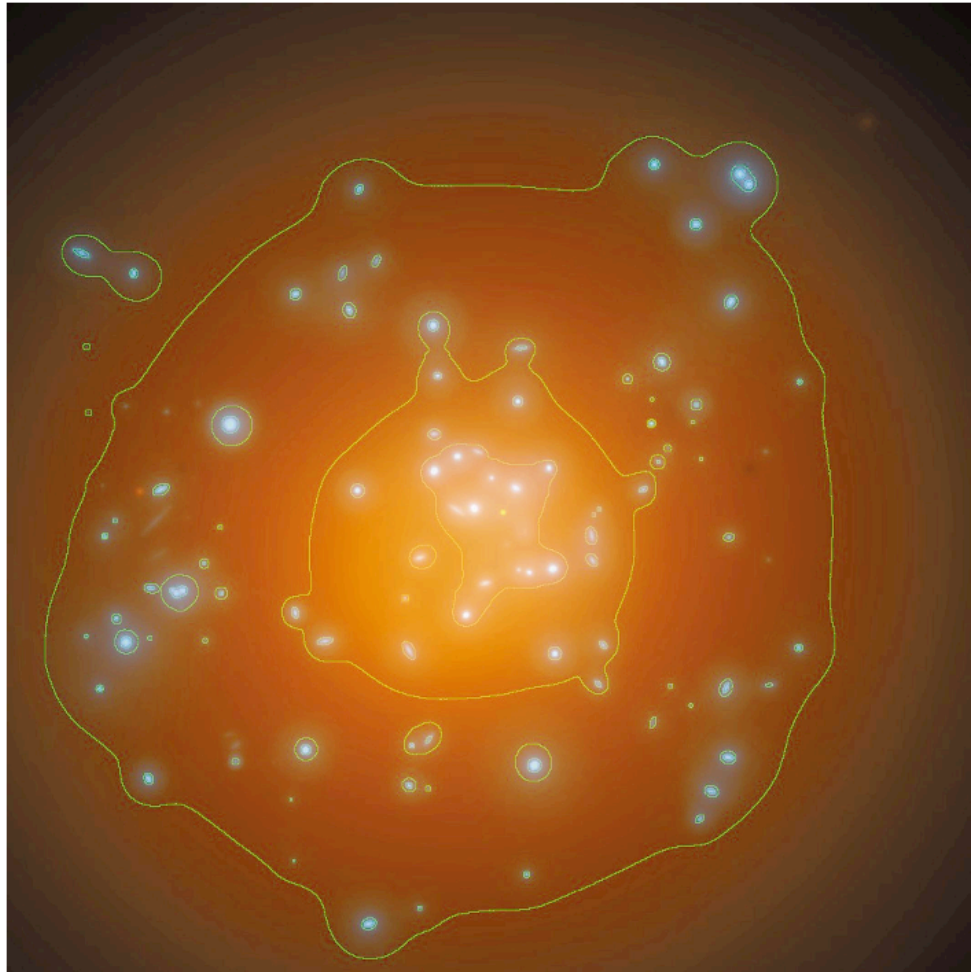
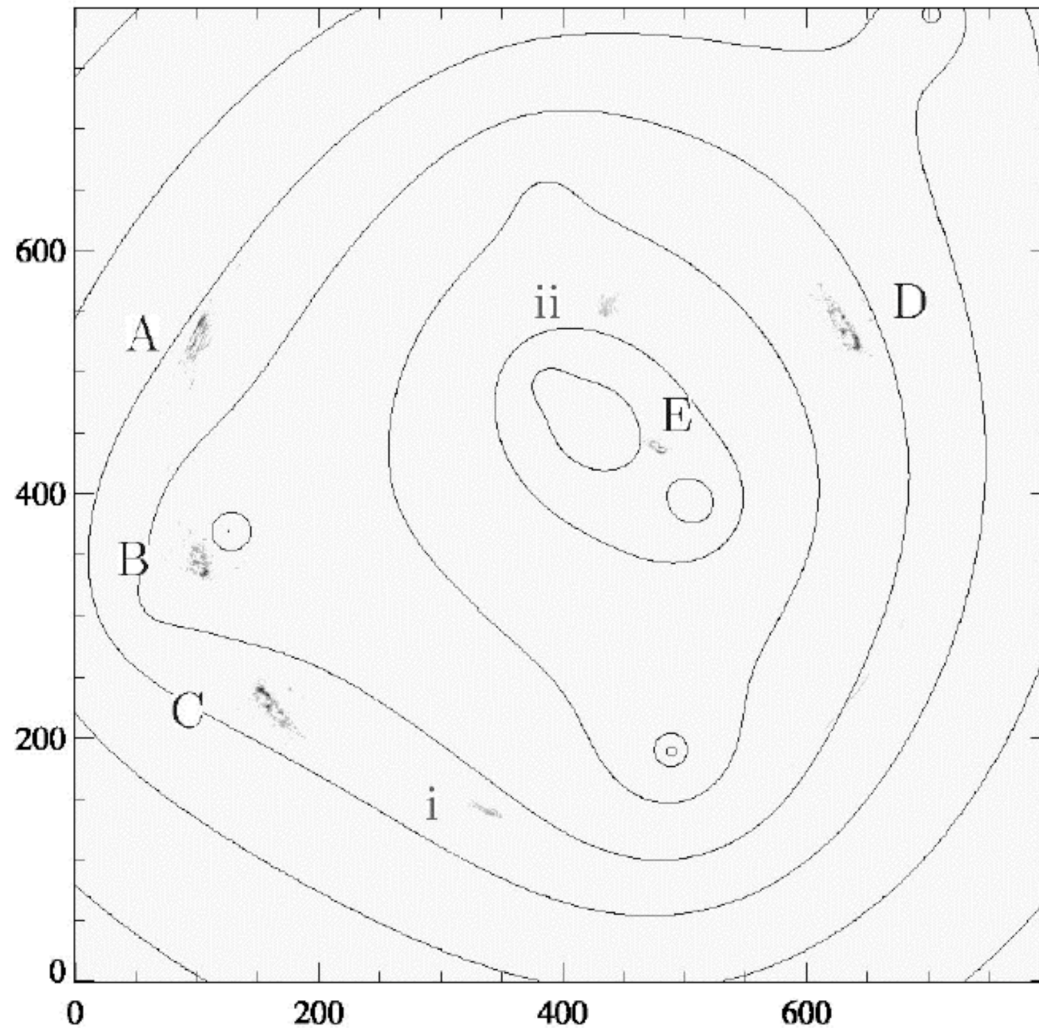


FIG. 1.—The reconstructed total mass density in CL 0024 is shown as a color-coded mass image. The DM is shown in orange. The mass associated with visible galaxies is shown in blue. The contours are at 0.5, 1, and 1.5 times the critical lensing density ($+197 h \sigma_{87}^{-1} M_{\odot} \text{pc}^{-2}$), with heavier contour at the critical lensing density. This image is $336 h^{-1} \text{kpc}$ across. North is up, and east is left.

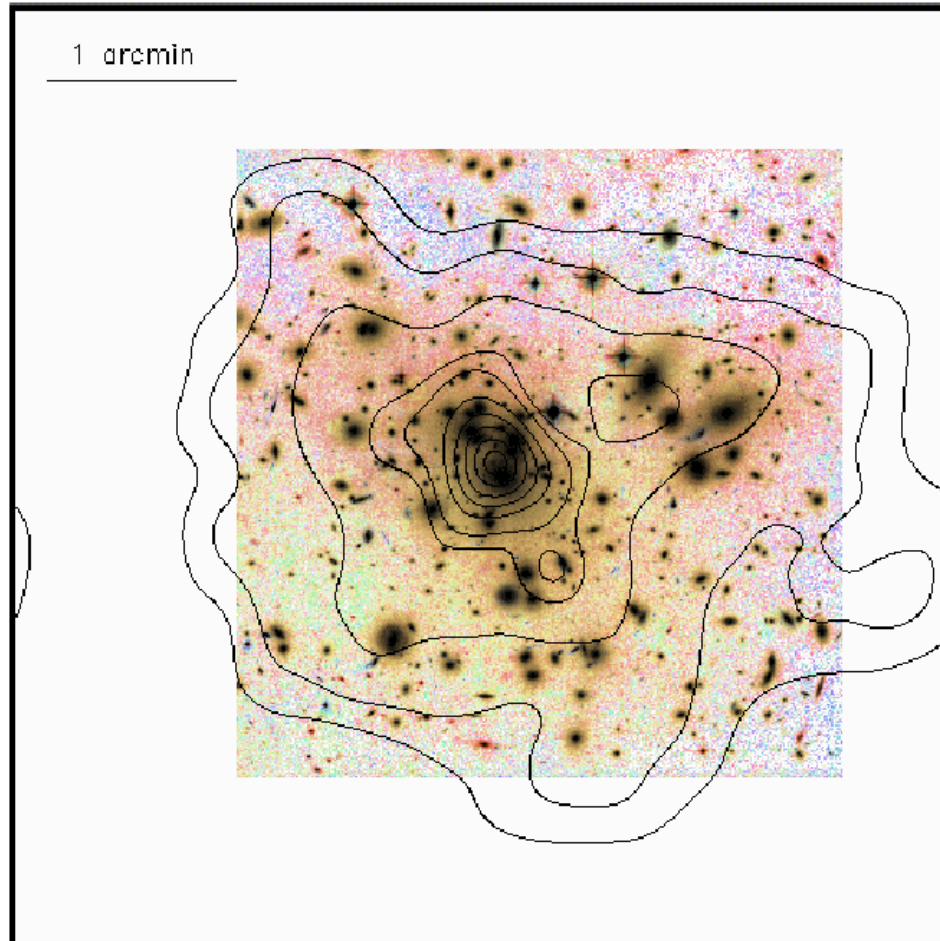
TYSON, KOCHANSEI, & DELL'ANTONIO (see 496, L108)

Broadhurst et al (2000)



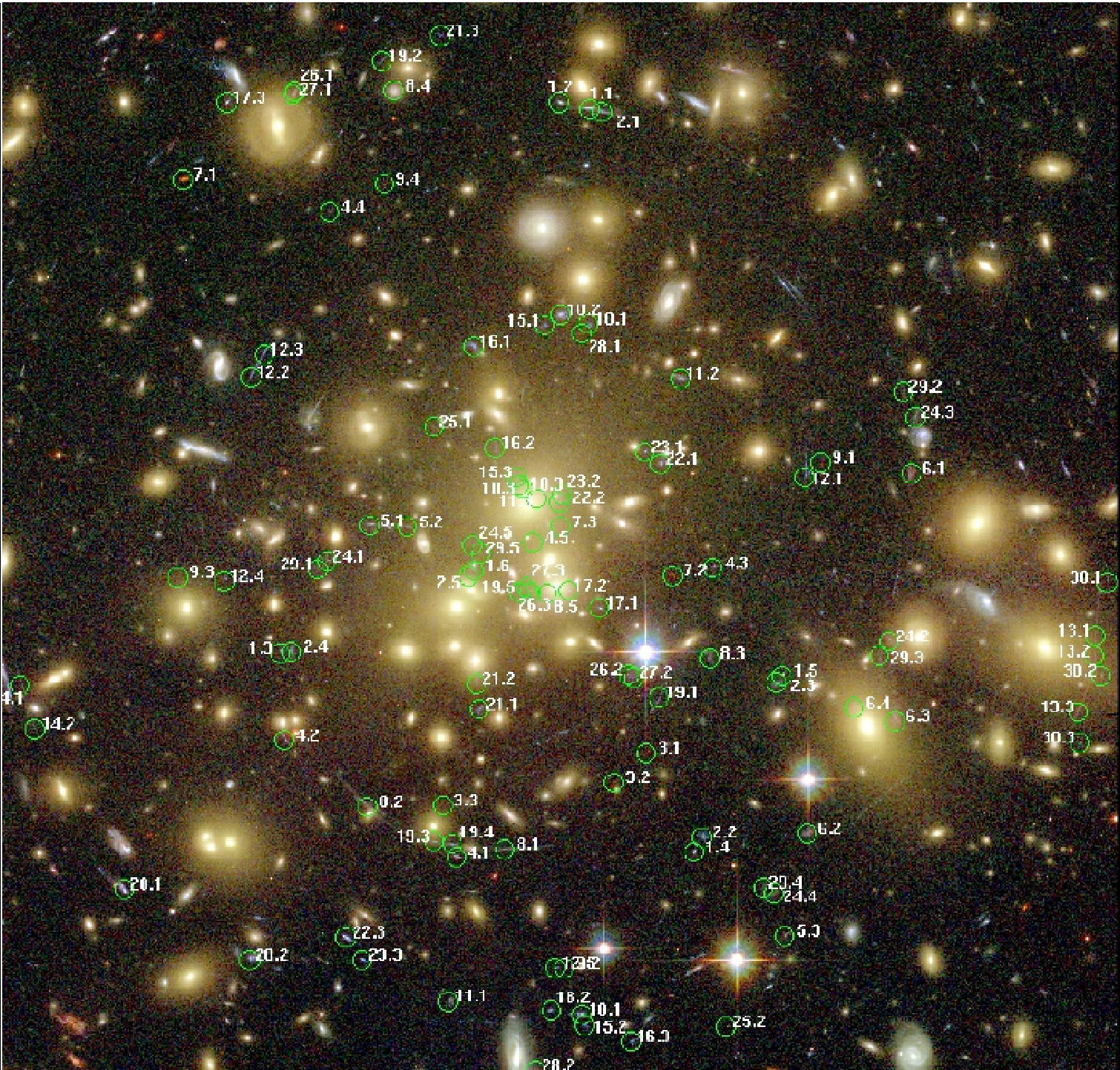
- Spectroscopic redshift for source galaxy
- Cluster mass profile consistent with NFW
- Significant substructure required

Diego, Sandvik, Protopas, Tegmark et al

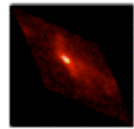


Non-parametric
Mass
reconstruction
of same cluster

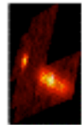
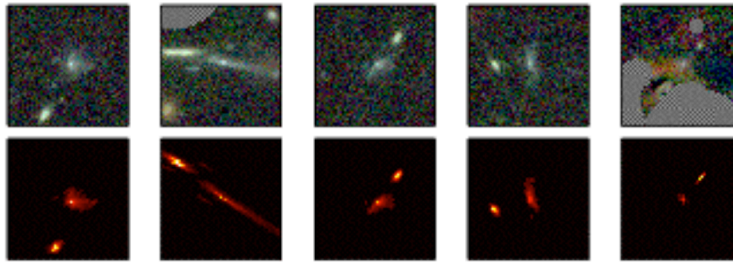
Reasonably good
agreement with
Broadhurst et
al mass model



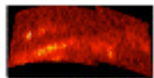
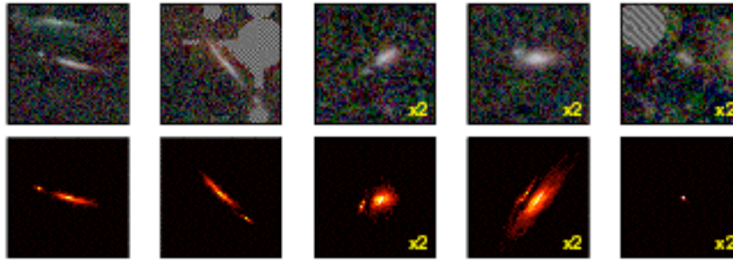
June 2



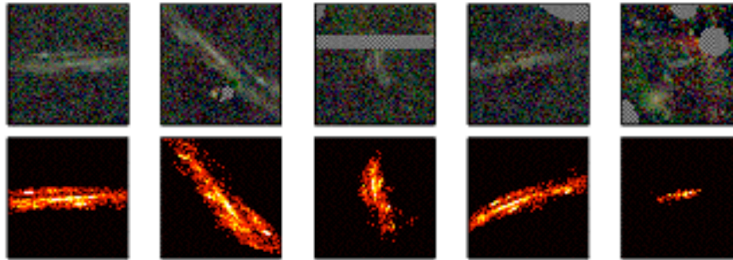
Source 2
x6.0



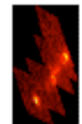
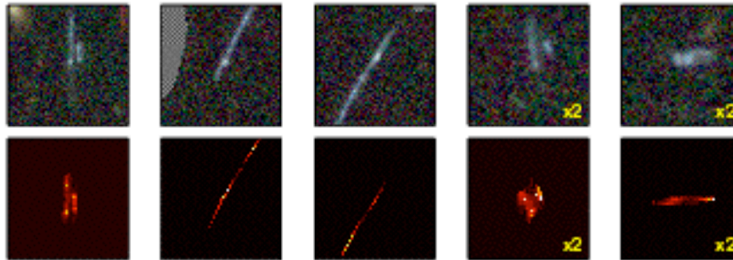
Source 4
x11.1



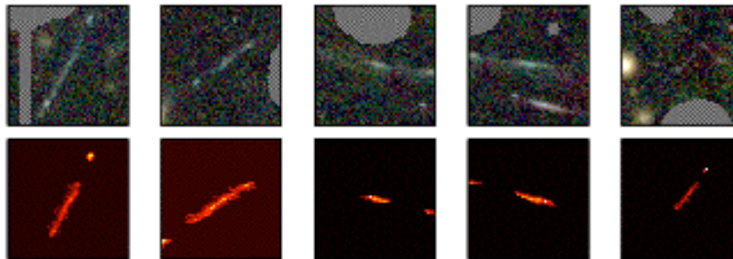
Source 8
x3.4



Source 12
x8.1



Source 19
x6.5



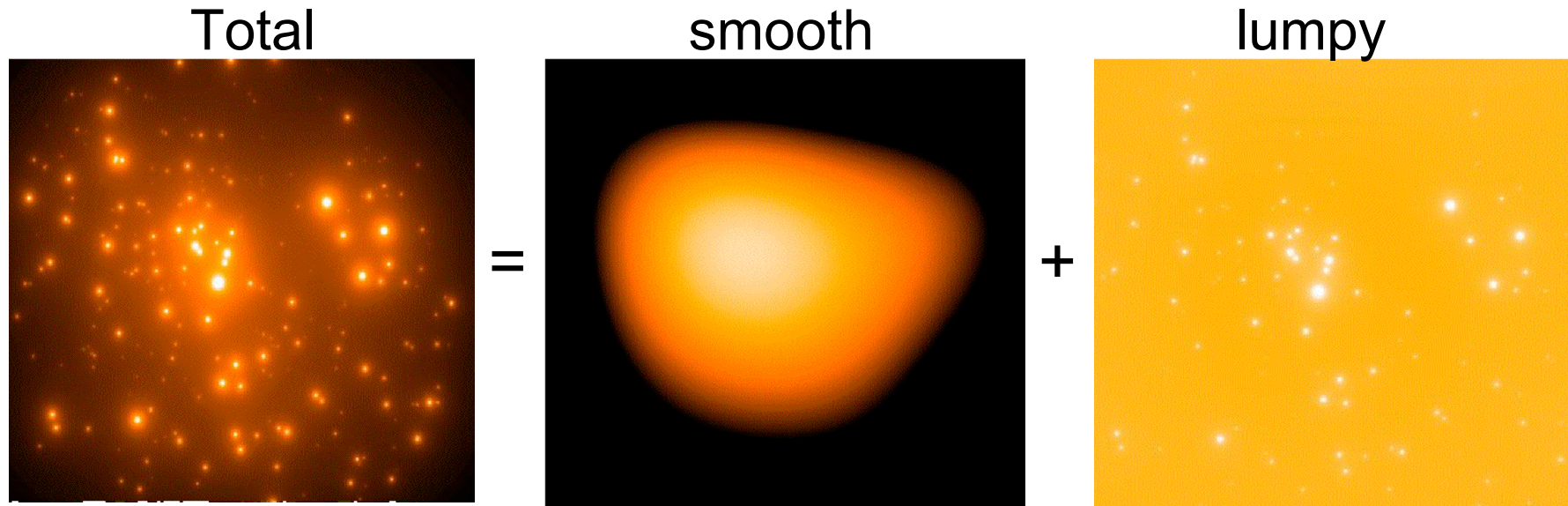
- All sources with five lensed images

- Leftmost panel shows reconstructed image of source (in source plane) generated by de-lensing the largest image (second column)

Mass Modeling and Raytracing

- “Our preference...is not to get bogged down in detail.”
- Start by assigning azimuthally symmetric power law surface density profile ($\Sigma \sim 1/r^q$) to 246 early type galaxies
- Bin mass on lens plane into 1024x1024 grid
- Fit smooth component with cubic spline
- Total deflection angle is sum of contributions from smooth cluster and lumpy galaxy mass distributions ($\alpha_T = \alpha_s + \alpha_g$)

Mass Modeling and Raytracing

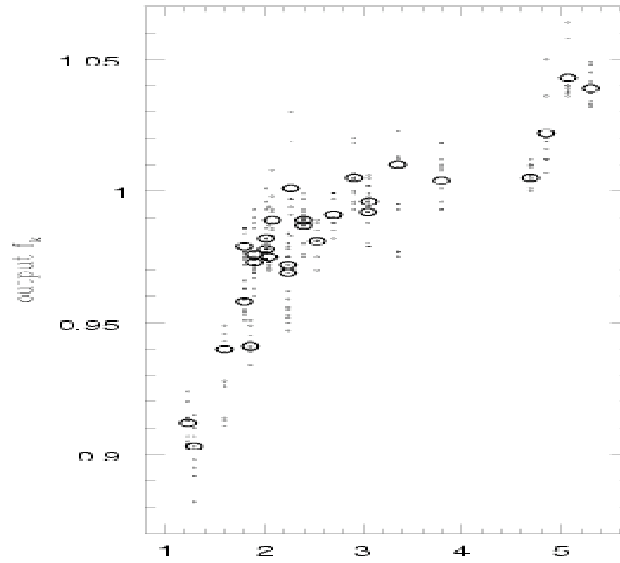
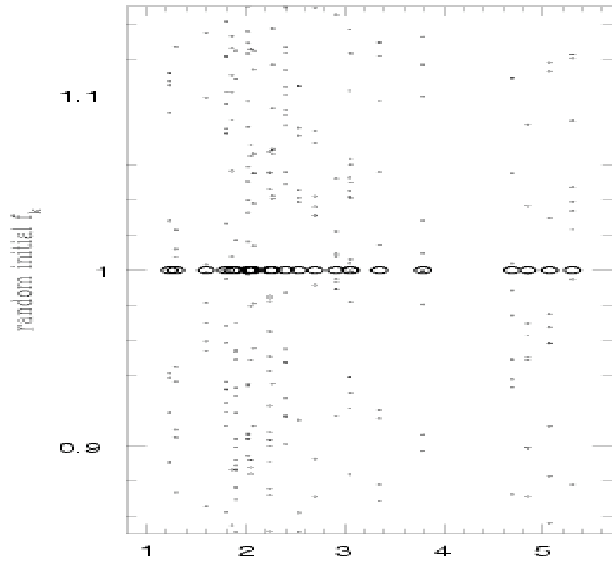


- Find best fit solution by iterating deflection fields, introducing polynomial perturbations to smooth component and two free parameters for amplitude of galaxy and smooth components

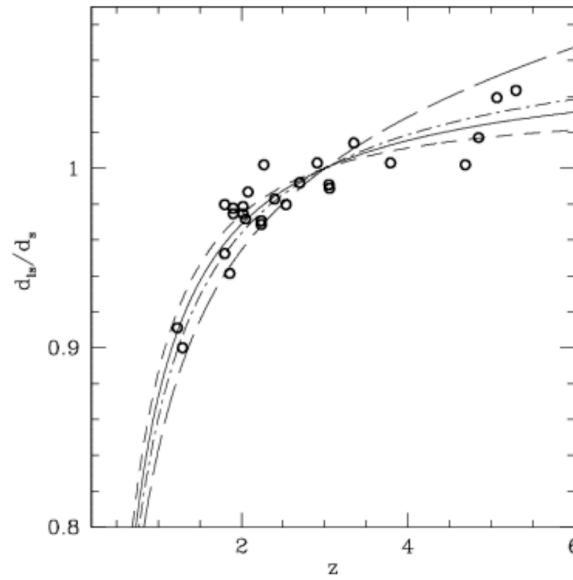
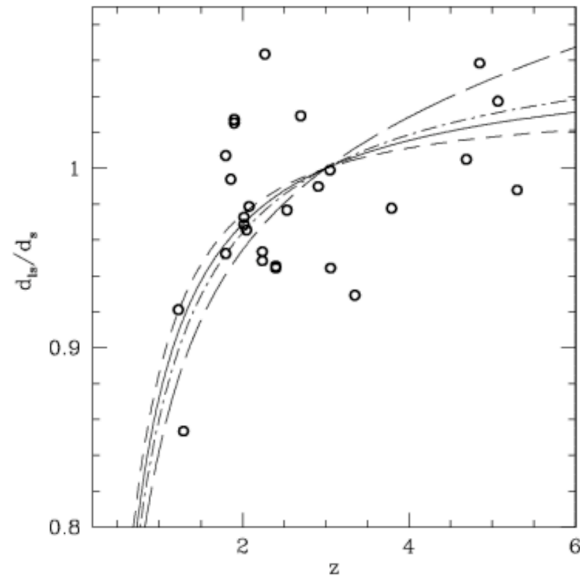
$$\alpha_{T-} = A_0((\alpha_{s-} + P) + R\alpha_{g-})$$

Mass Modeling and Raytracing

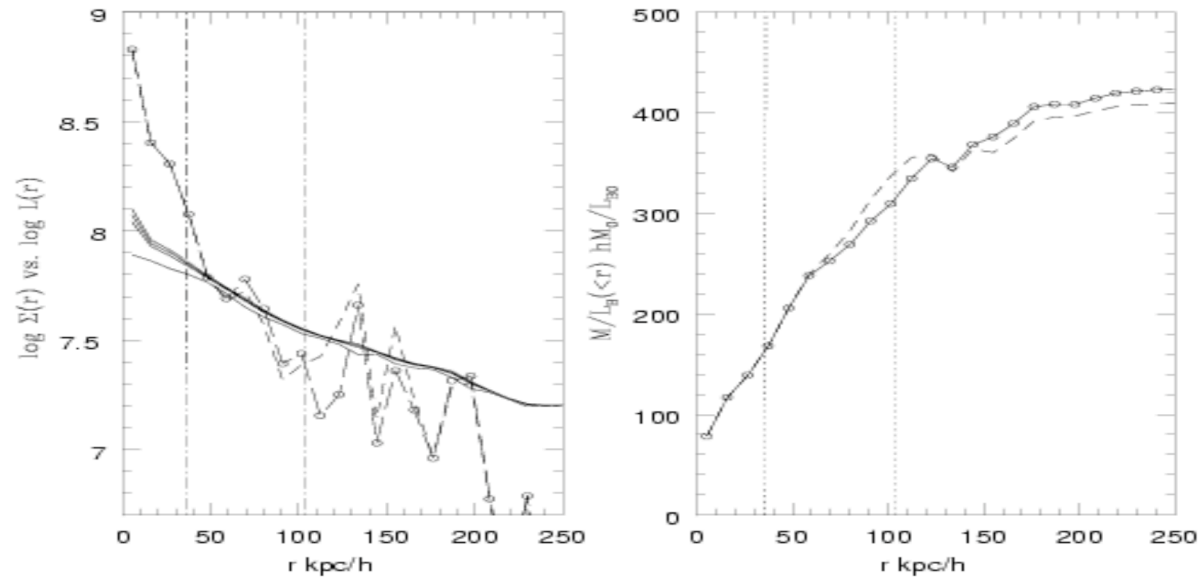
- Minimization of difference between observed image positions and image positions predicted by raytracing through mass model
- Angular diameter distance ratio of each source scales amplitude of deflection fields, but so does normalization of surface density distribution
 - i.e., mass and geometry (cosmology) determine α
 - Initially assume redshift of $z=3$ for all sources
- Downhill simplex method used to find minimum χ^2 solution



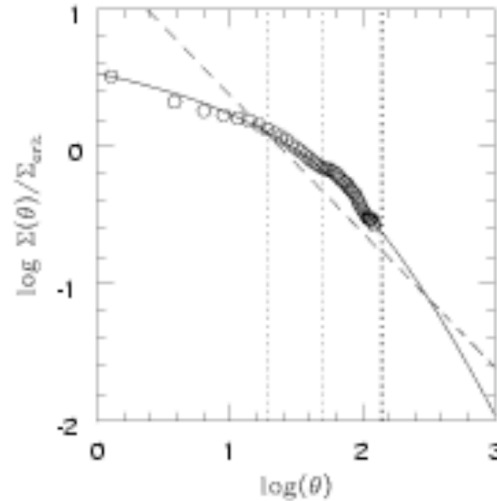
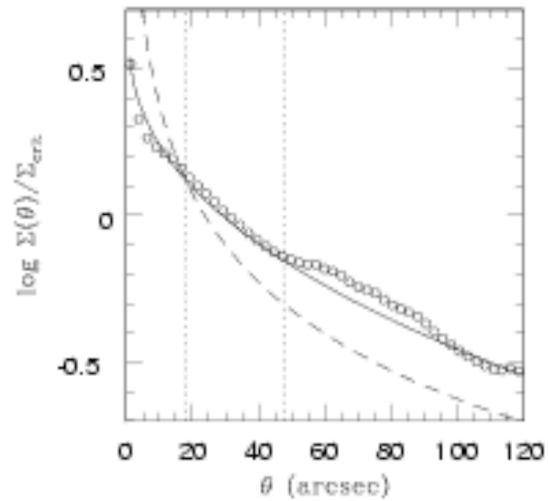
$$f_k = \frac{D_k(z)}{D_k(z=3)}$$



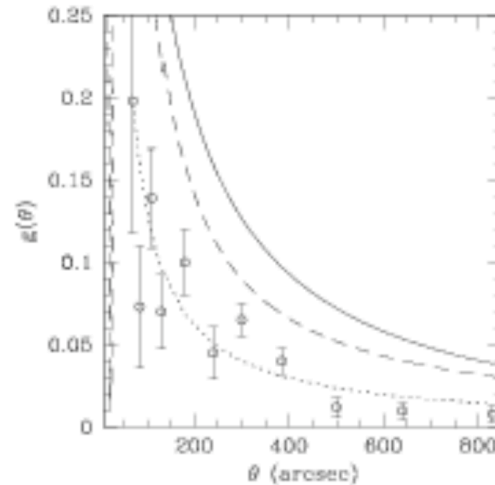
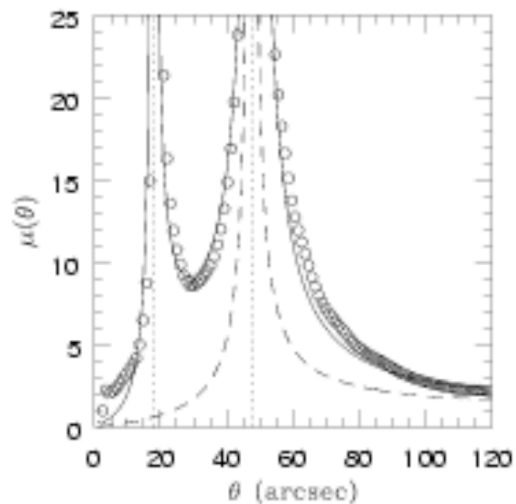
Ω_M	Ω_L
0.1	1.2
1.0	
0.3	0.7
0.1	0



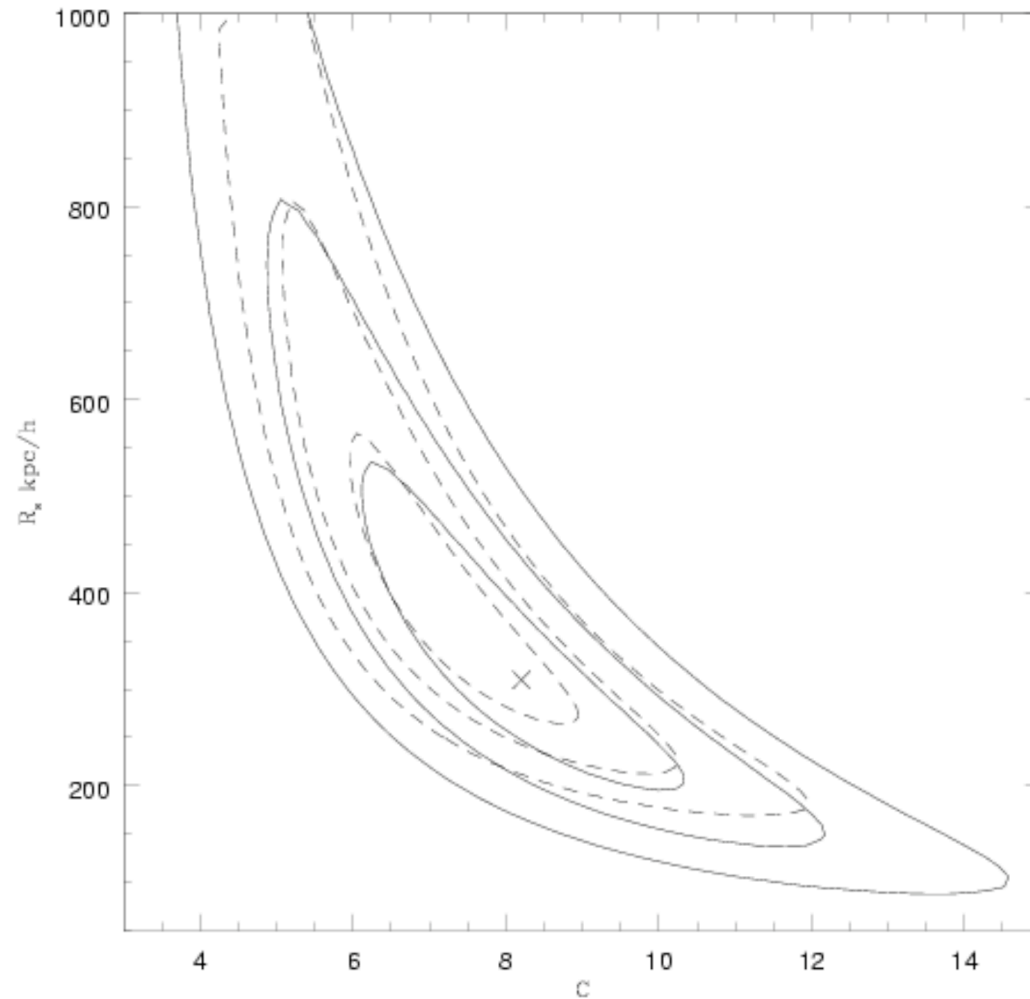
- comparison with light map
 - light more concentrated than mass within $r < 50 \text{ kpc}/h$



Solid = NFW
Dashed = isothermal



Lower right: factor of ~2 discrepancy between these results and weak lensing results of Clowe and Schneider for A1689



Concentration of
NFW fit is
 $C = 8.2 + 2.1 / - 1.8$

Compared to
 $C \sim 5 + / - 2$ for
CDM cluster
halos

Diego, Sandvik, Protopas, Tegmark et al

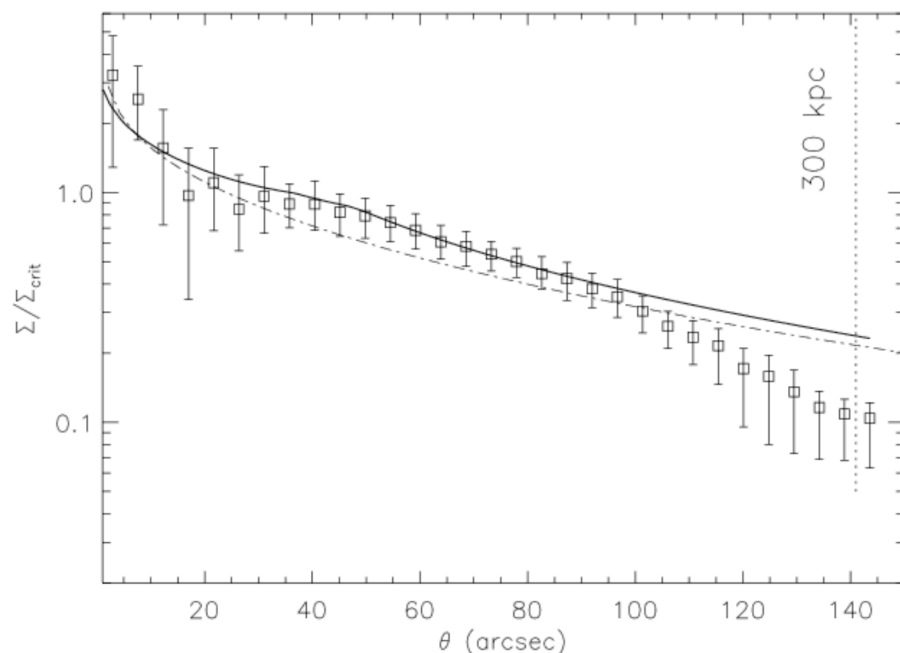


Figure 4. The plot shows the mean value (squares) and the 99% confidence region of the 1D profiles for the 1000 minimizations in case *i*). The dot-dashed line is the best fitting NFW profile found in B2004. The density has been rescaled by the critical density, Σ_{crit} . The thick solid line is a very similar NFW profile plus an excess given by 3 NFW subhaloes around the main halo. See text

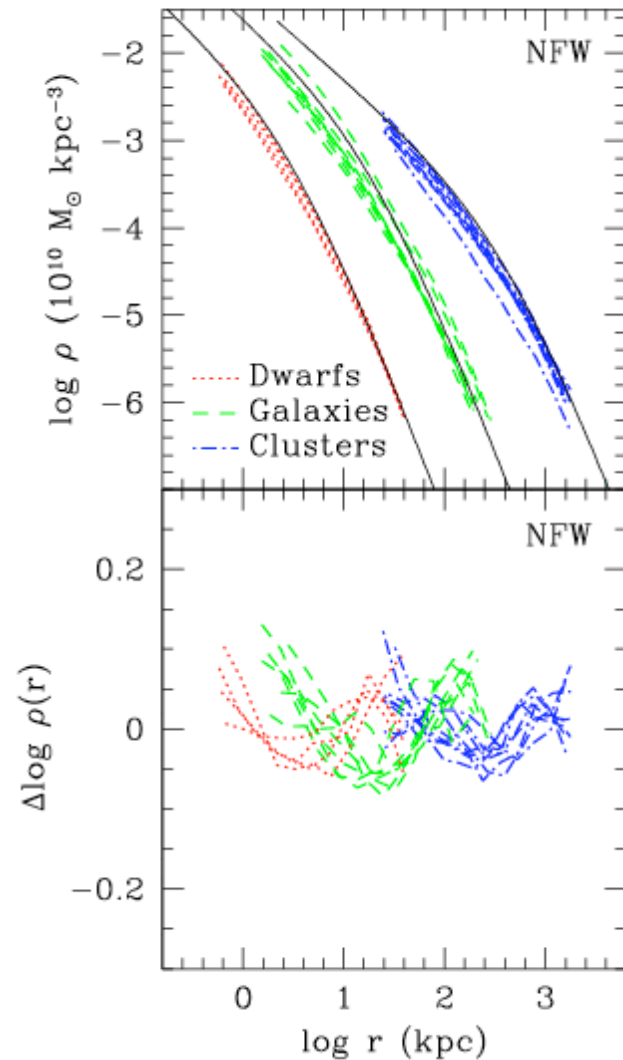
Non-parametric
Mass
reconstruction
of same cluster

Reasonably good
agreement with
Broadhurst et
al mass model

Summary

Don't leave things until the last minute...

Global Deviations from NFW Profile



- NFW profile does a reasonably good job of fitting halo profiles over the region resolved by simulations

- NFW profile turns over too sharply at $r < r_s$, resulting in a poor fit near the centre

- Largest deviations from NFW range from 10-25%

Tyson, Kochanski & Dell'Antonio (1998)

- HST imaging of multiply lensed background galaxy in cluster CL 0024+1654
- Dark and luminous components of galaxy cluster modeled with spherical mass concentrations
- Light from reconstructed source galaxy raytraced through lens plane mass model
- Resulting image compared with observed image

Reconstructed Mass Map of CL 0024

- Reconstructed cluster mass density

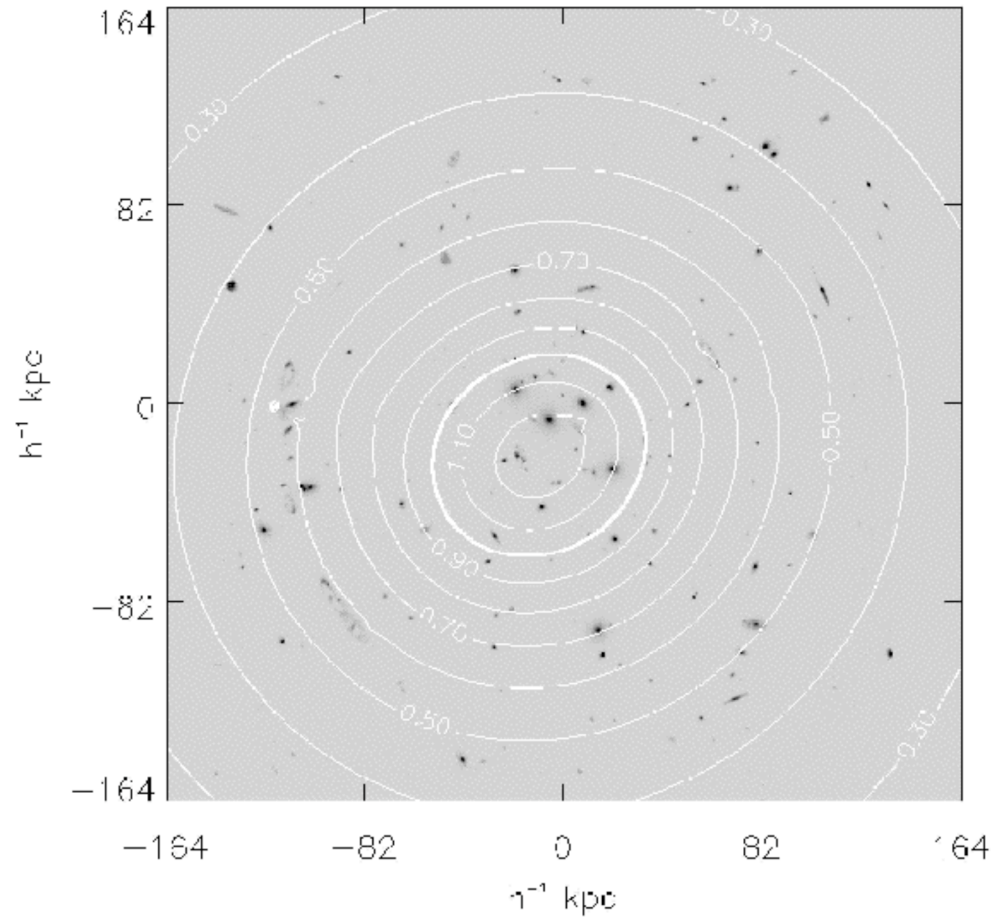


FIG. 2.—The reconstructed mass density not associated with visible galaxies in CL 0024 is shown as a contour plot (white contours), superposed on the F450W (blue) *HST* image for reference. Iso-mass contours for this dark mass are at $0.1\sigma_c$ intervals in projected mass density, with a thick contour at $1\sigma_c$, as labeled. The plot is $336 h^{-1}$ kpc ($100''$) across, centered at R.A. = $00^{\text{h}}23^{\text{m}}56^{\text{s}}$, decl. = $16^{\circ}53'15''$ (1950). On scales larger than 10 kpc, this majority component of the DM is remarkably smooth. The DM substructure has already been erased by $z = 0.39$.

Reconstructed Mass Map of CL 0024

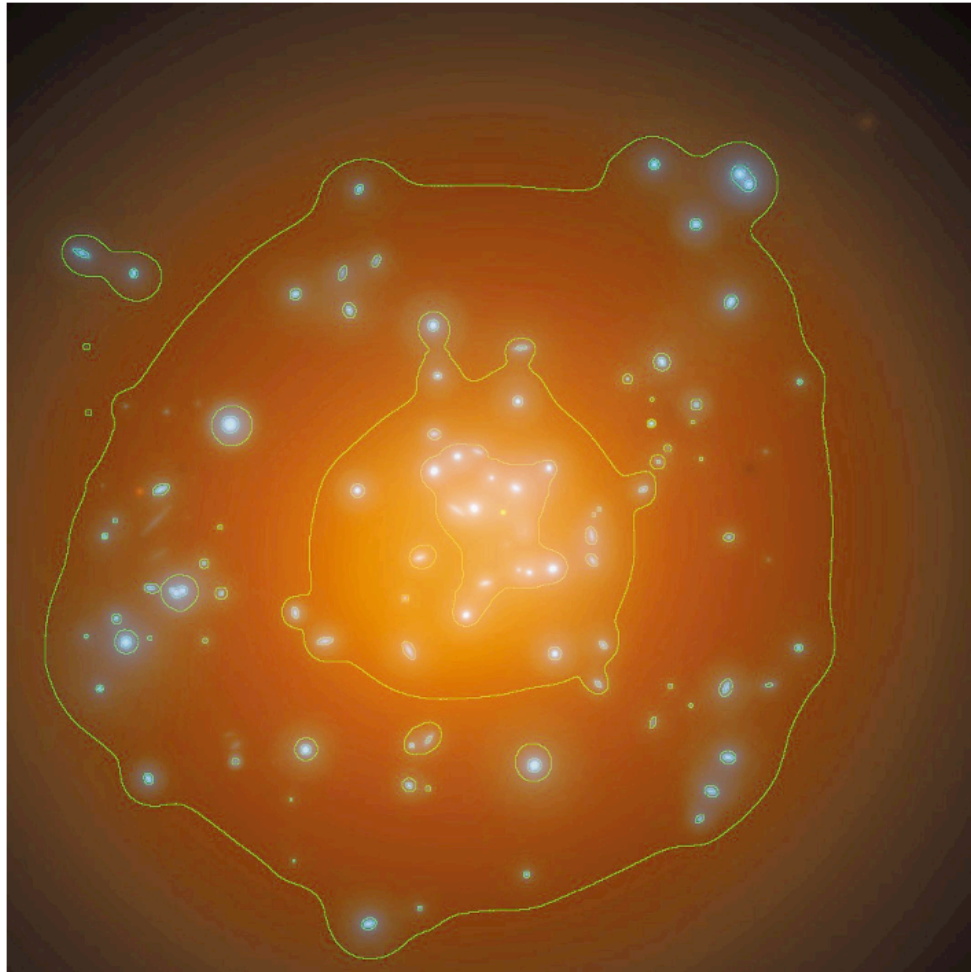
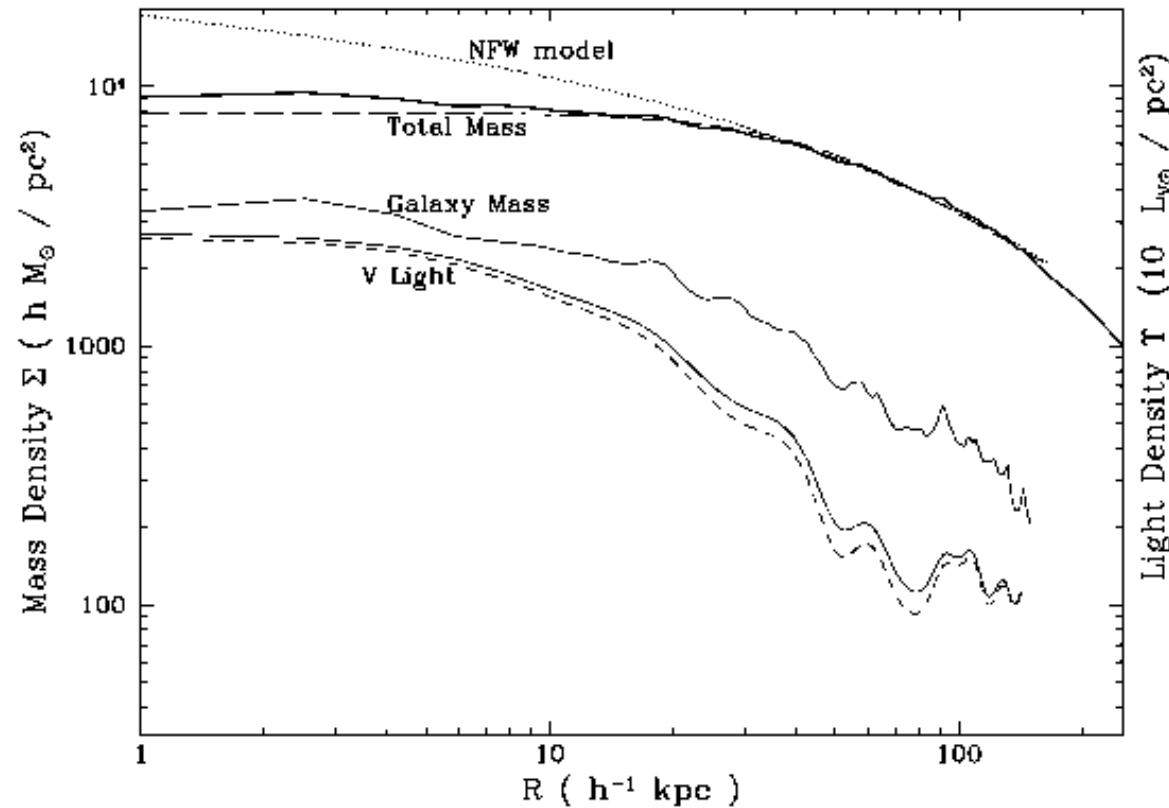


FIG. 1.—The reconstructed total mass density in CL 0024 is shown as a color-coded mass image. The DM is shown in orange. The mass associated with visible galaxies is shown in blue. The contours are at 0.5, 1, and 1.5 times the critical lensing density ($+197 h \sigma_{87}^{-1} M_{\odot} \text{pc}^{-2}$), with heavier contour at the critical lensing density. This image is $336 h^{-1} \text{kpc}$ across. North is up, and east is left.

TYSON, KOCHANSEI, & DELL'ANTONIO (see 496, L108)

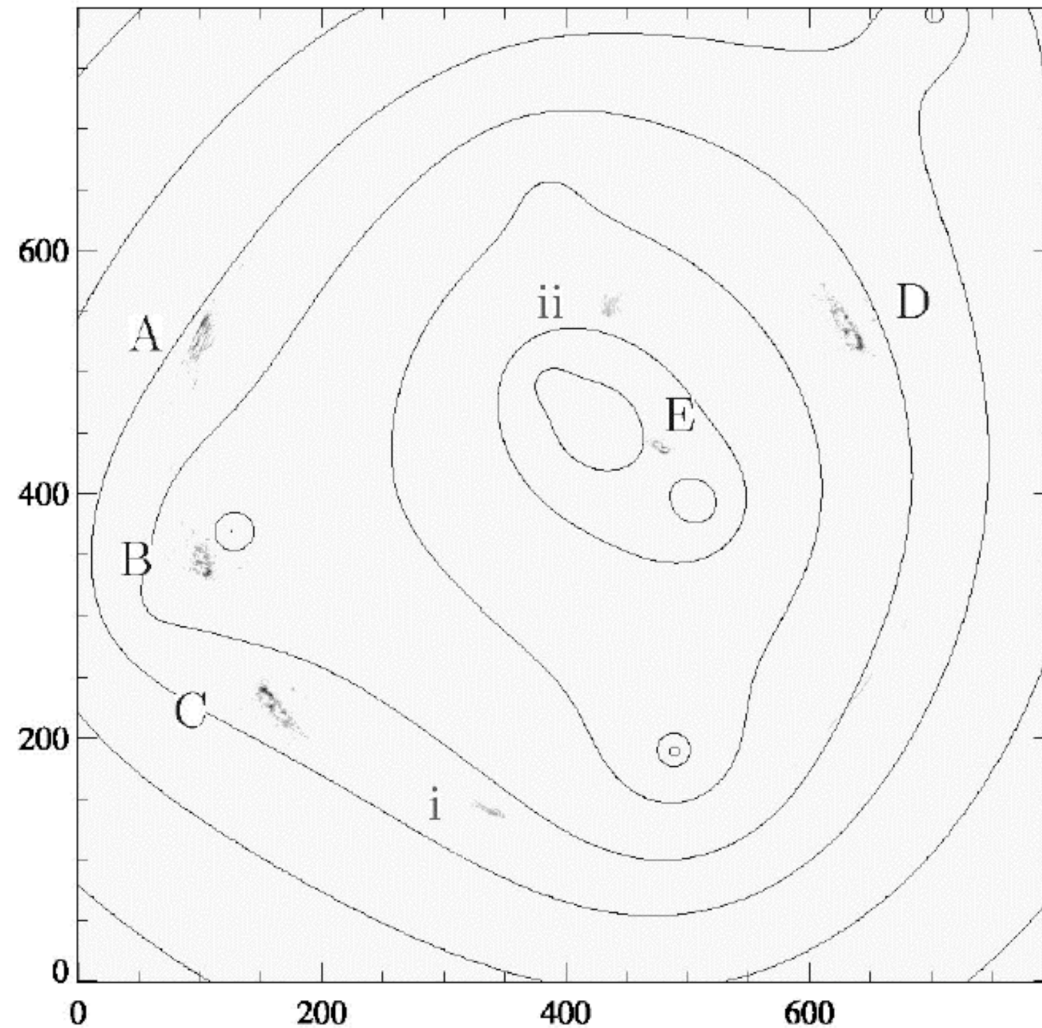
Mass Profile of CL 0024



- DM mass density profile has a 35 kpc/h “soft core” (chewy centre?)
- Not consistent with singular density profiles like NFW

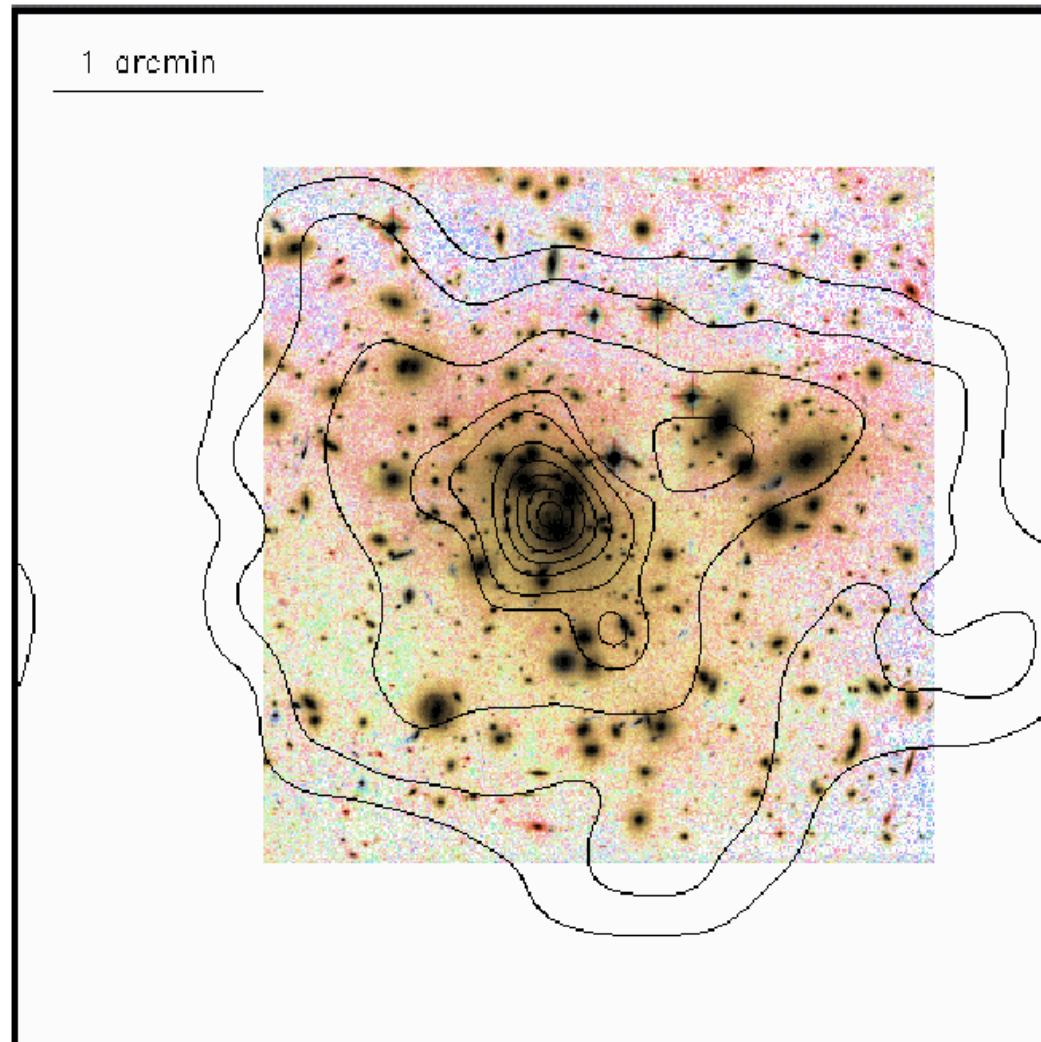
-A radial plot of the mass density and light density. Total (*thick line*) and galaxy-only (*thin line*) components of the mass are shown. The dotted line NFW fit discussed in the text, and the dashed line is the best-fit single PL model. The 35 h^{-1} kpc soft core in the mass is evident. A singular mass profile is ruled out. The total rest-frame V light profile (*solid line*) and galaxy V light profile (*dashed line*), smoothed with a 5 h^{-1} kpc Gaussian, are also

Broadhurst et al (2000)



- Spectroscopic redshift for source galaxy
- Cluster mass profile consistent with NFW
- Significant substructure required

Broadhurst et al (2000)



- Spectroscopic redshift for source galaxy
- Cluster mass profile consistent with NFW
- Significant substructure required

Sand, Treu & Ellis (2002)

- Dark matter density profile of galaxy cluster MS 2137-23 ($z=0.313$)
- Obtained imaging and spectroscopy of Brightest Cluster Galaxy (BCG) and of radial and tangential arcs
- 1D lensing analysis and stellar velocity dispersion of BCG used to constrain mass profile of cluster

Spectroscopy of BCG and Arcs

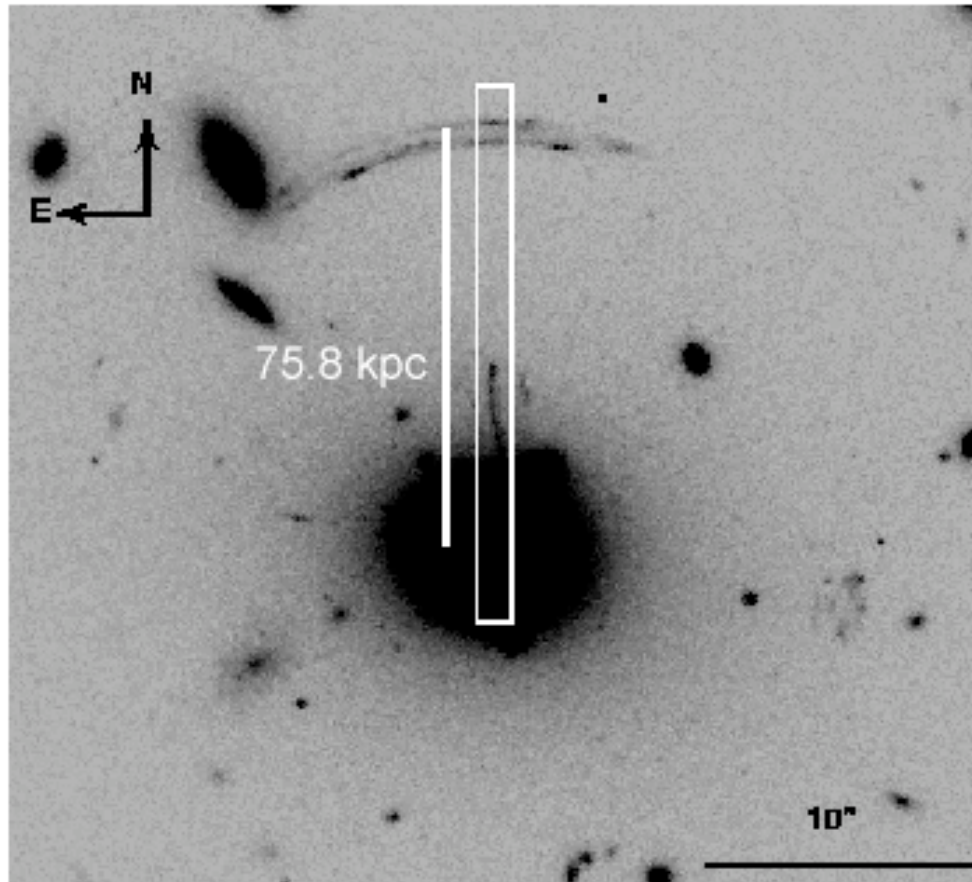
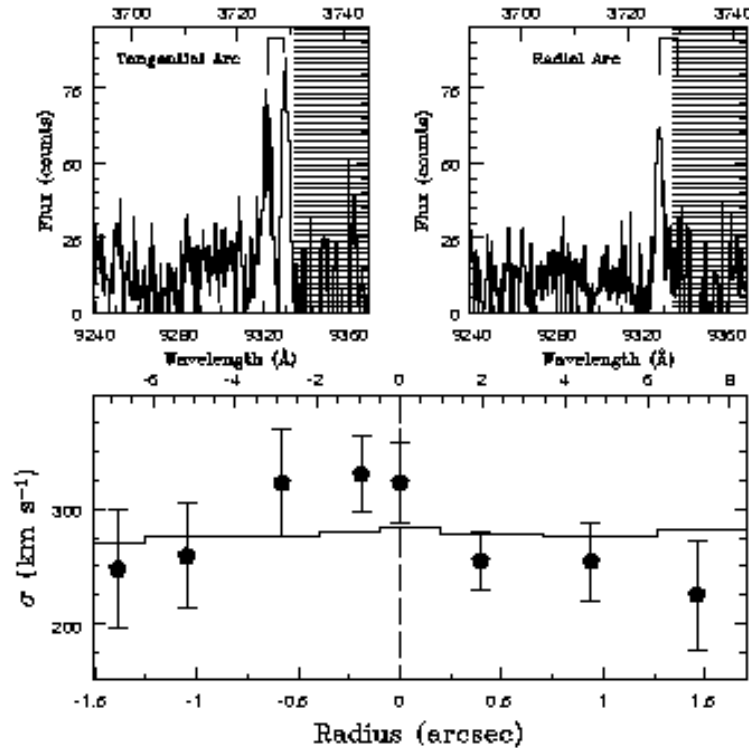


FIG. 1.— HST F702W image of MS2137-23. The rectangular box shows the dimensions ($1''.25 \times 20''$) and position of the ESI slit used to make the observations. The BCG, the radial and tangential arc are clearly visible at the bottom, center, and upper end of the slit.

- Obtained spectra of BCG and radial and tangential arcs using Echelle Spectrograph Imager on Keck II
- Used HST imaging to measure photometry of BCG and positions of arcs

Spectra of Arcs and Velocity Dispersion of BCG



- [OII] doublet identified in arc spectra gives $z=1.501$ and $z=1.502$ for tangential and radial arcs
- Velocity dispersion profile of BCG measured using stellar spectral templates of G-K giants

FIG. 2.— Spectroscopic results: (Top) Strong emission lines detected in the spectra of the tangential and radial arcs. These are identified as [OII]3726,3729 at $z = 1.501$ and $z = 1.502$ respectively (marked). It is argued that the missing 3729 Å line in the radial arc is obscured by sky emission. (Bottom) Stellar velocity dispersion profile of the brightest cluster galaxy (points with error bars). The superimposed histogram shows the profile of the best fitting Jaffe + generalized NFW mass model (see Sec. 3 for details), taking into account the effects of seeing ($0''.6$), slit width, and radial binning.

Lensing Mass Model

- Spherical 2-component mass model
- Jaffe density profile for luminous component:

$$\rho_L(r) = \frac{M_L r_J}{4\pi r^2 (r_J + r)^2}$$

- Generalized CDM halo density profile:

$$\rho_d(r) = \frac{\rho_{crit} \delta_c}{(r / r_{sc})^\beta (1 + r / r_{sc})^{3-\beta}}$$

- 4 free parameters: 1) M_*/L_V , 2) inner slope β , 3) DM density d_c , 4) DM scale radius r_{sc}

Constraints on DM inner slope

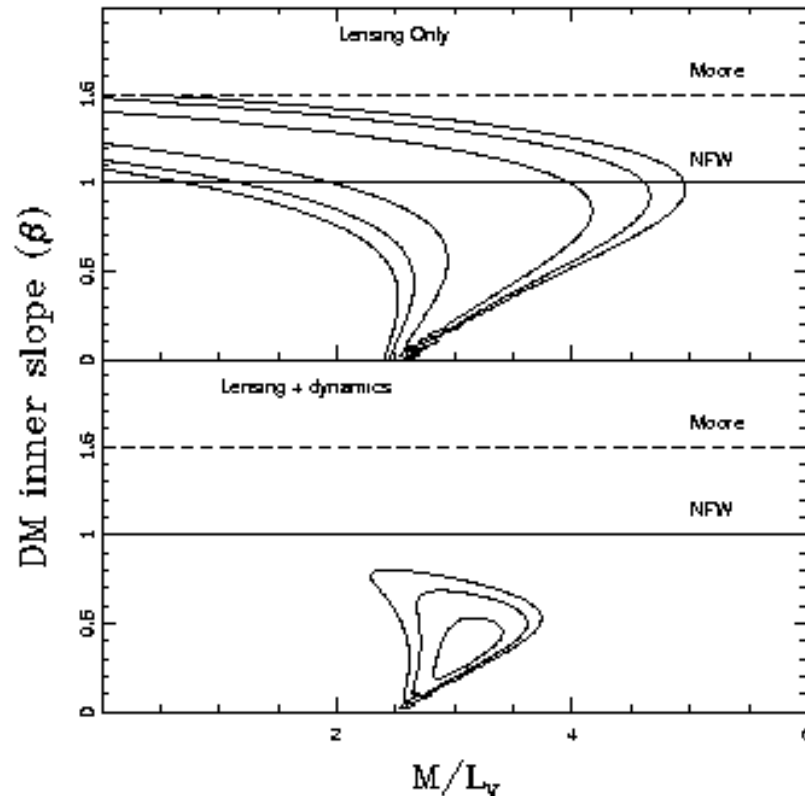


FIG. 3.— Likelihood contours (68%, 95%, and 99%) obtained for the mass modeling of MS2137-23 with a Jaffe luminous distribution plus a generalized NFW DM distribution. (Top): Contours obtained from the position of the radial and tangential arcs alone. Note that a Moore ($\beta = 1.5$) profile is excluded at the 95% level. (Bottom): Contours obtained including the measured velocity dispersion profile. Note the improved constraints on the mass parameters and that NFW profiles are clearly ruled out at the 99% level.

- Constructed lensing likelihood function by comparing observed positions of arcs and predicted positions for a given mass model
- “Dynamics” likelihood function based on velocity dispersion profile derived using spherical Jeans equation assuming isotropic velocity ellipsoid

Sand, Treu & Ellis (2003)

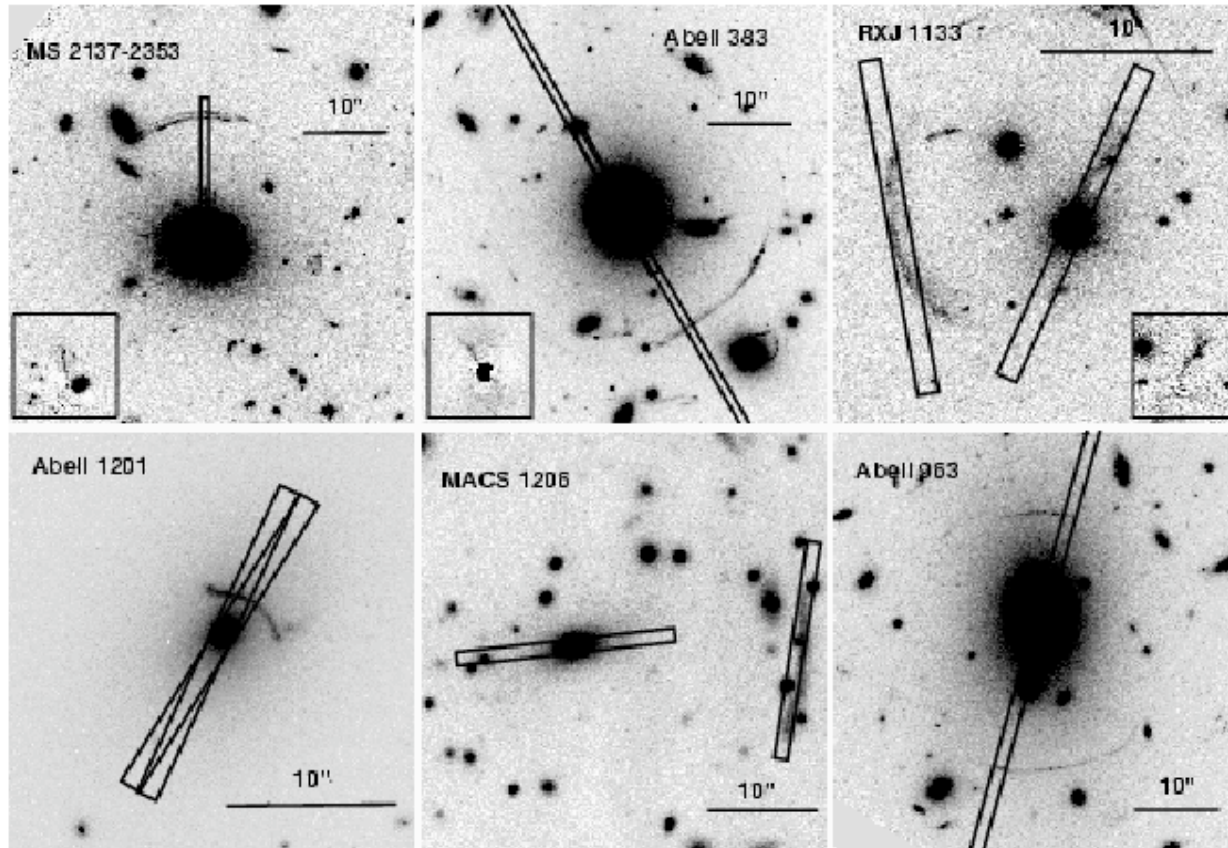


FIG. 1.— Images of the six clusters in this study. The top row features the clusters with both radial and tangential arcs. The postage stamp insets show zoomed in BCG subtracted images so that the radial arcs can be clearly seen. The bottom row contains those clusters with tangential arcs only. The overlaid “slits” correspond to the actual slit positions and sizes that were observed. See Table 3 for the spectroscopic observation log. North is up and East is to the left in all images.

- Performed same analysis on five more clusters
- Top row: clusters with radial **and** tangential arcs
- Bottom row: clusters with tangential arcs only

Constraints on Inner Slope

$$\beta = 0.57^{+0.11}_{-0.08} \quad \beta = 0.38^{+0.06}_{-0.05} \quad \beta = 0.99^{+0.18}_{-0.14}$$

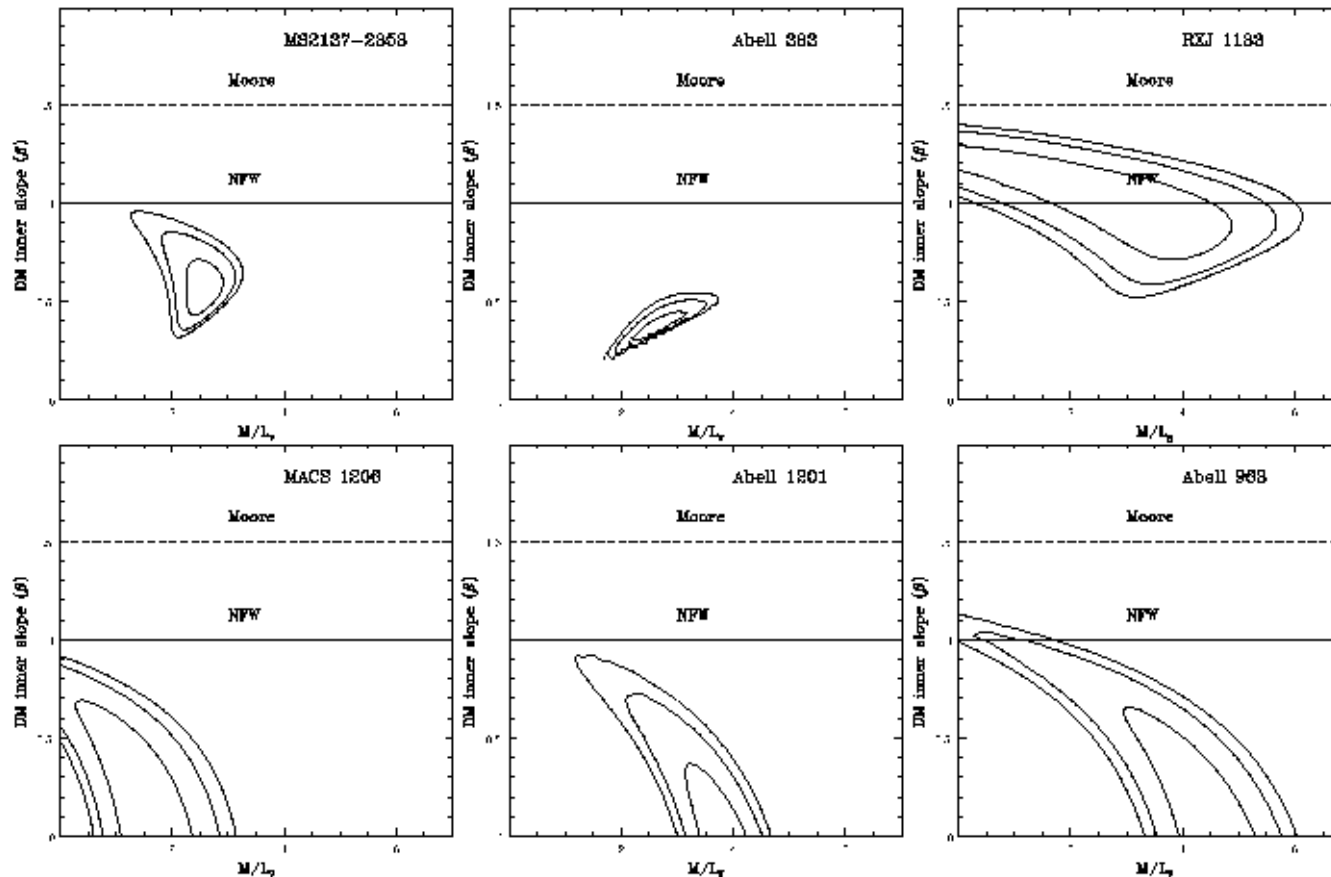
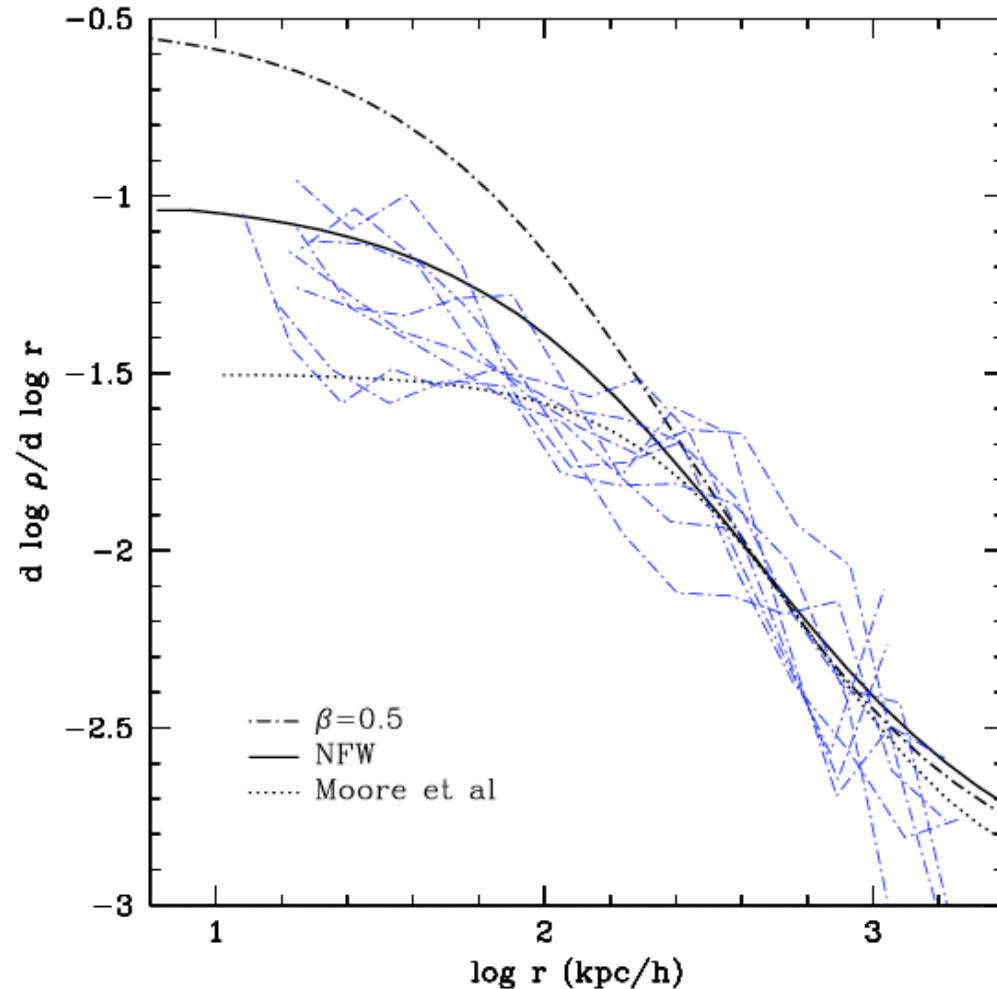


FIG. 3.— Likelihood contours (68%, 95% and 99%) obtained for the radial arc sample (top row) and the tangential arc sample (bottom row) with a Jaffe luminous distribution plus a generalized NFW DM distribution. These contours were obtained after both the lensing and dynamical analysis and marginalization with respect to δ_c .

- Average inner slope of clusters with radial arcs is $\beta = 0.52^{+0.05}_{-0.05}$ (68% CL)
- Clusters with tangential arcs only give upper limit of $\beta < 0.57$ (99% CL)

Log Slope of N-Body Cluster Halos



- Average slope of simulated clusters at innermost resolved radius is $\beta \approx 1.2 \gg 0.5$
- Simulations and observations have comparable scatter, $\Delta\beta \sim 0.3$

Probability Distribution Functions

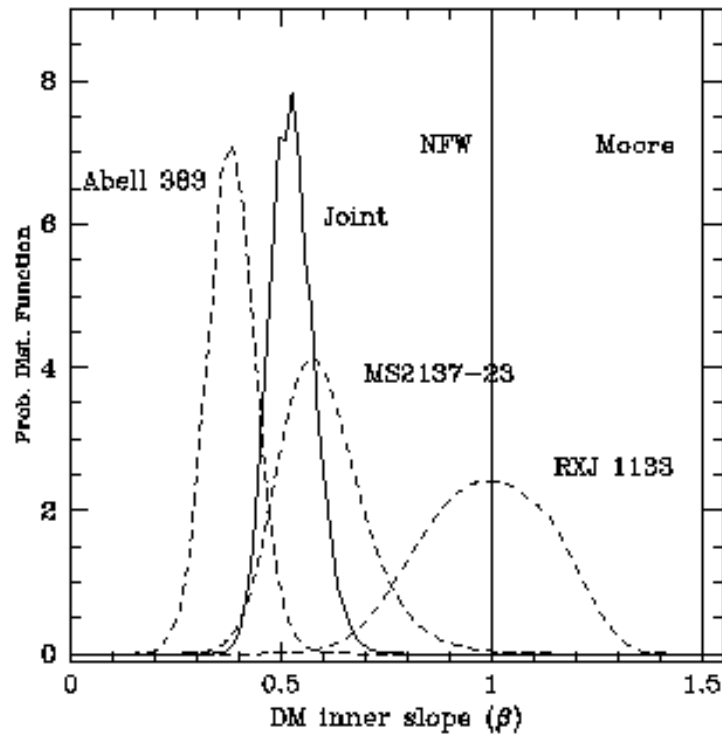


FIG. 4.— Probability distribution function of the DM inner density slope, β , for the three radial arc clusters. Note the wide scatter in preferred values of β from cluster to cluster, $\Delta\beta \sim 0.3$. The joint distribution was obtained by multiplying the individual PDFs and normalizing.

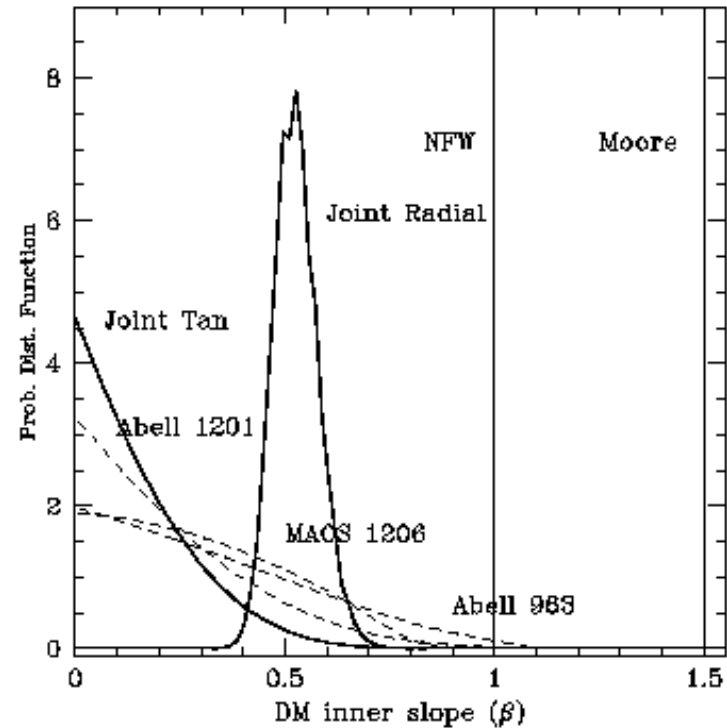


FIG. 5.— Probability distribution function of the DM inner density slope, β , for the tangential arc sample. These effectively allow us to place an upper limit on β for each cluster. Also plotted is the joint PDF for the radial arc sample and the tangential arc sample. There is no evidence that the radial arc sample is biased towards lower values of β .

- Mean DM distribution of all 6 clusters is inconsistent with $\beta=1$ at $> 99\%$ CL

Systematic Effects

Systematic	Test	$\Delta\beta$
Cluster ellipticity and substructure	Used LENSTOOL ray-tracing program to construct non-spherical mass model for clusters with radial and tangential arcs	0.2
Anisotropic velocity distribution in BCG	Introduced constant radial and tangential anisotropy in calculation of BCG velocity dispersion	0.2
Choice of luminous mass model	Used Hernquist model instead of Jaffe	Negligible
BCG surface photometry fits	Changed effective radius by +/- 10%	Negligible

Strong Lensing in Galaxy Clusters

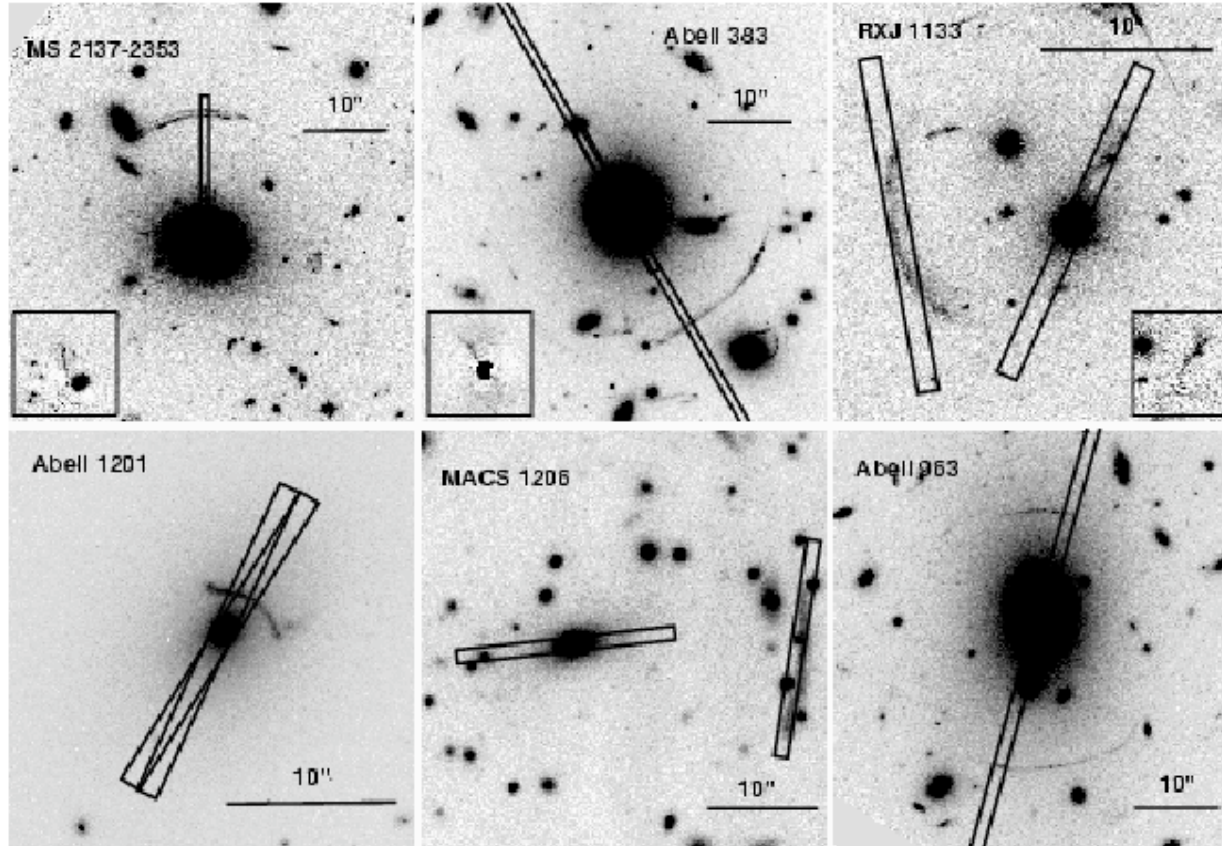
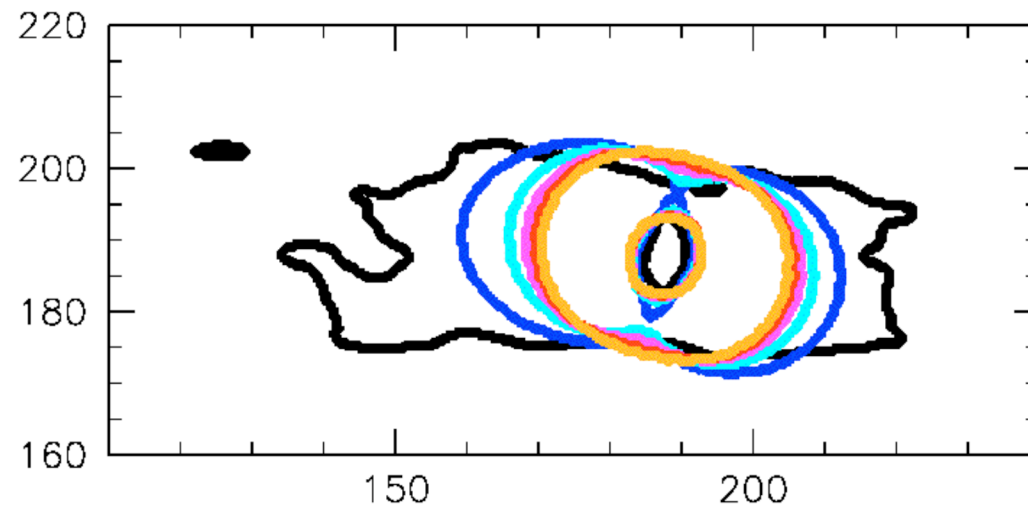


FIG. 1.— Images of the six clusters in this study. The top row features the clusters with both radial and tangential arcs. The postage stamp insets show zoomed in BCG subtracted images so that the radial arcs can be clearly seen. The bottom row contains those clusters with tangential arcs only. The overlaid “slits” correspond to the actual slit positions and sizes that were observed. See Table 3 for the spectroscopic observation log. North is up and East is to the left in all images.

- Sand, Treu & Ellis (2003): used gravitational lensing and stellar dynamics to constrain mass profiles of six galaxy clusters
- Mean cluster density profile is inconsistent with NFW at 99% CL
- See Bartelmann & Meneghetti and Dalal & Keeton for effects of ellipticity

Deviations from Axial Symmetry



- Reconstructed cluster mass density

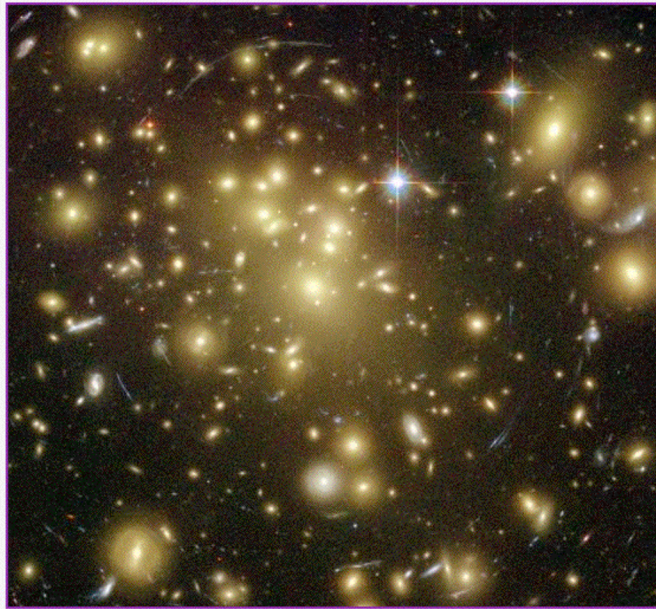
Fig. 5. Critical curves of a simulated cluster in various stages of smoothing. As described in the text, the smoothing procedure conserves the total cluster mass and its density profile by construction. The ragged line is the original critical curve. Even moderate smoothing makes the critical curves shrink and considerably reduces the radial range where tangential and radial arcs can be found.

Abell 1689

Astronomy Picture of the Day

[Discover the cosmos!](#) Each day a different image or photograph of our fascinating universe is featured, along with a brief explanation written by a professional astronomer.

2004 June 27



Galaxy Cluster Abell 1689 Warps Space

Credit: [N. Benitez \(JHU\)](#), [T. Broadhurst \(Hebrew Univ.\)](#), [H. Ford \(JHU\)](#), [M. Clampin \(STScI\)](#),
[G. Hartig \(STScI\)](#), [G. Illingworth \(UCO/Lick\)](#), [ACS Science Team](#), [ESA](#), [NASA](#)

Explanation: Two [billion](#) light-years away, galaxy cluster Abell 1689 is one of the most massive objects in the Universe. [In this view](#) from the Hubble Space Telescope's [Advanced Camera for Surveys](#), Abell 1689 is seen to warp space as predicted by [Einstein's](#) theory of gravity -- bending light from individual galaxies which lie behind the cluster to produce multiple, curved images. The power of this [enormous](#) gravitational lens depends on its mass, but the [visible matter](#), in the form of the cluster's yellowish galaxies, only accounts for about one percent of the mass needed to make the observed [bluish arcing images](#) of background galaxies. In fact, most of the gravitational mass required [to warp space](#) enough to explain this cosmic scale lensing is in the form of still mysterious [dark matter](#). As the dominant source of the cluster's gravity, the [dark matter's](#) unseen presence is [mapped out](#) by the lensed arcs and [distorted](#) background galaxy images.

Tomorrow's picture: [red hills of mars](#)

- HST ACS imaging of Abell 1689 by Broadhurst et al (2004)

Summary

Q: Is there a conflict between observations and theory?

A: Maybe.



Summary

Q: Is there a conflict between observations and theory?

A: Maybe.

Simulations with sufficient resolution to resolve down to 10 kpc/h contain dark matter only (no baryonic physics). However, the inclusion of baryons is expected to steepen the density profile, making the problem even worse. Perhaps a more complicated interaction between baryonic material and dark matter which forms the central cusp..?

- As usual, more observations and simulations are necessary before CDM can be ruled out..

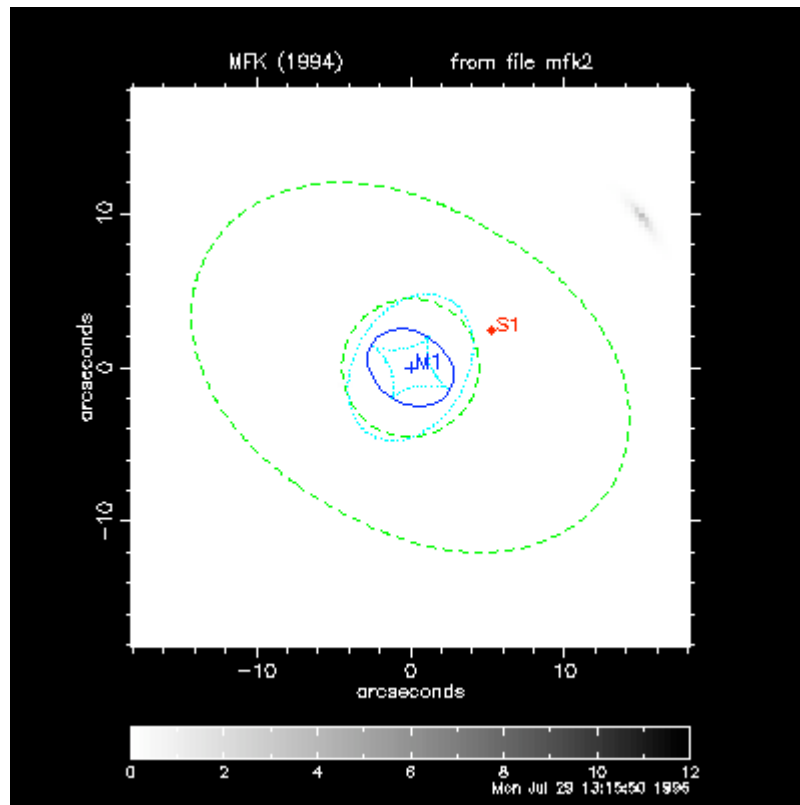
Summary

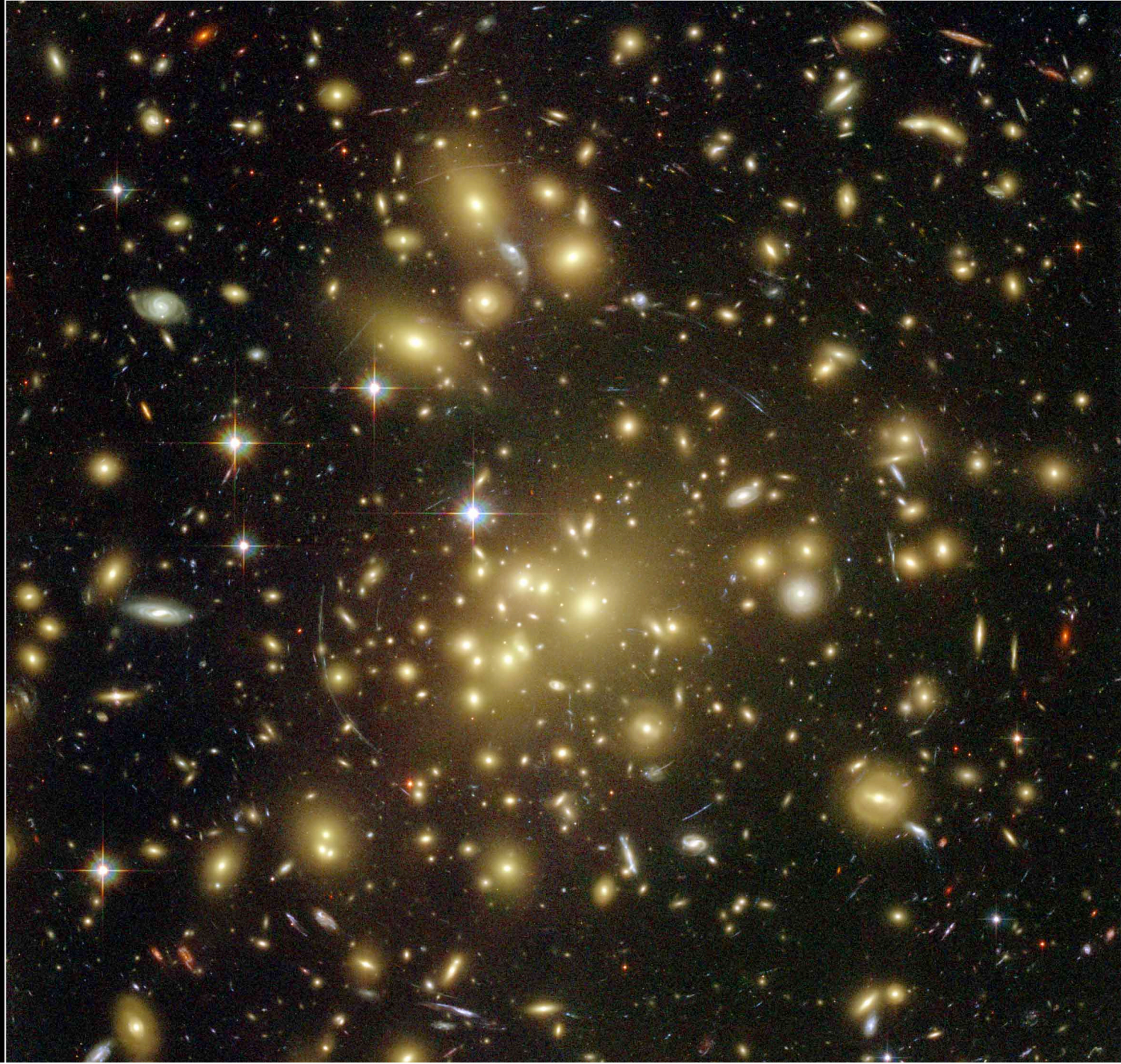
- As usual, more observations and simulations are necessary before CDM can be ruled out..

The End

June 2 2005

Trieste Conference





Galaxy Cluster Abell 1689

Hubble Space Telescope • Advanced Camera for Surveys

ASA, N. Benitez (JHU), T. Broadhurst (The Hebrew University), H. Ford (JHU), M. Clampin (STScI),
J. Hartig (STScI), G. Illingworth (UCO/Lick Observatory), the ACS Science Team and ESA
TScI-PRC03-01a

Introduction

Q: What is the nature of the Universe?

A: A Universe dominated by Cold Dark Matter (CDM) and nonzero Cosmological Constant Λ ?

- **Successes/Motivations:**
 - Clustering properties of CDM, CMB power spectrum, BBN and baryon fraction in clusters, supernovae cosmology
- **Challenges:**
 - Too much substructure in CDM halos?
 - Constant density “core” inferred from rotation curves
 - Distribution of mass on large scales from gravitational lensing

Testing the Paradigm

- What are the predictions of the model?
 - The structure of CDM halos in cosmological simulations
- Are the predictions consistent with observations?
 - The mass profile of galaxy clusters inferred from gravitational lensing studies
- “The ultimate test of theory lies in agreement with observations”

Hayashi, 2001

Dark Halo Structure: Then...

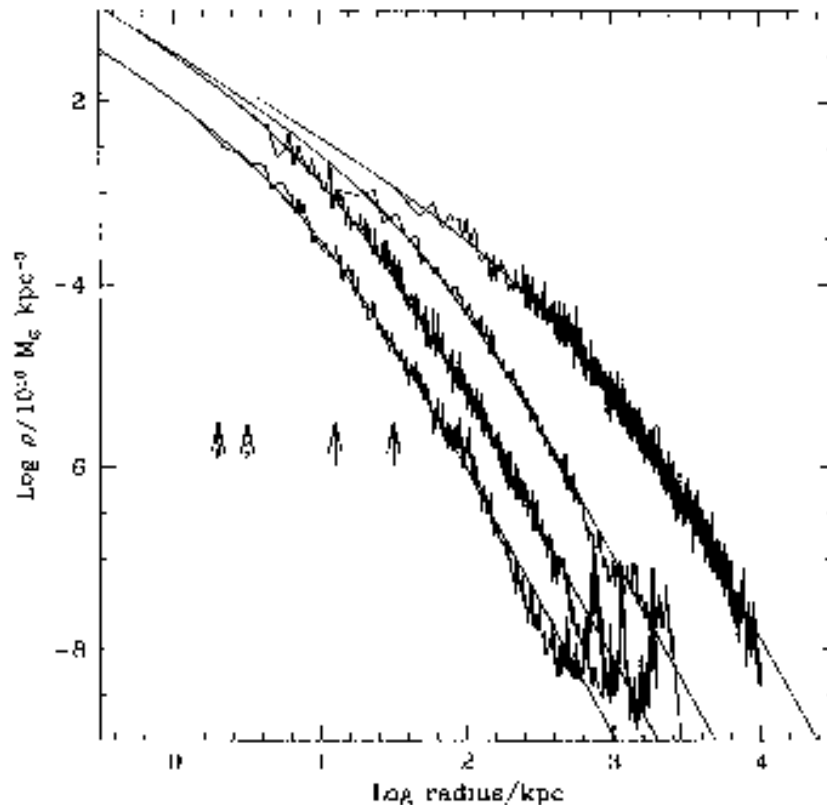


FIG. 3.—Density profiles of four halos spanning 4 orders of magnitude in mass. The arrows indicate the gravitational softening, h_p , of each simulation. Also shown are fits from eq. (3). The fits are good over two decades in radius, approximately from h_p out to the virial radius of each system.

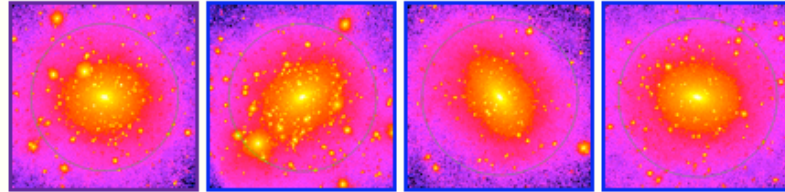
- Navarro, Frenk and White (NFW, 1996): a universal density profile of dark matter halos

$$\rho_{NFW} = \frac{\rho_{crit} \delta_c}{r / r_s (1 + r / r_s)^2}$$

- Inner slope of NFW profile is $\beta=1$
- Halos with 10^4 particles resolved down to 10% of virial radius, r_{vir}

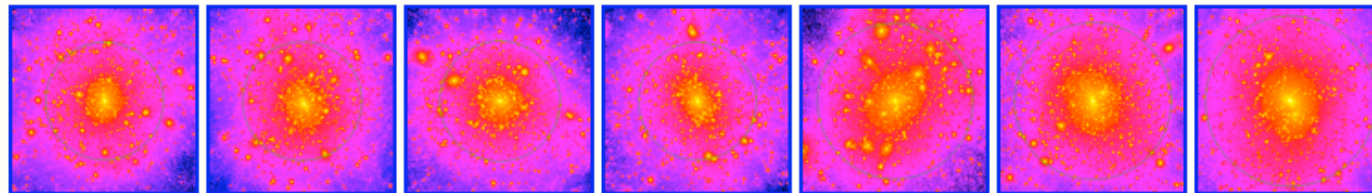
Dark Halo Structure: ...and Now

4 Dwarf Halos (80 kpc/h box shown)



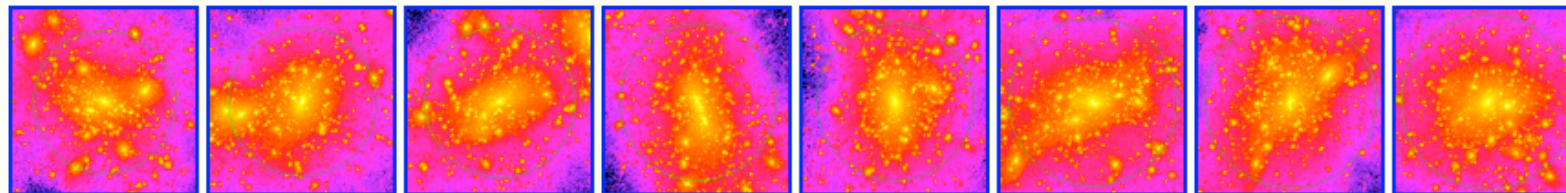
Halo1 Halo4 Halo2 Halo5

7 Galaxy-Sized Halos (500 kpc/h box shown)



ghxxx09 gh1_360 ghxxx08 ghxxx04 Halo3 Halo1 Halo2

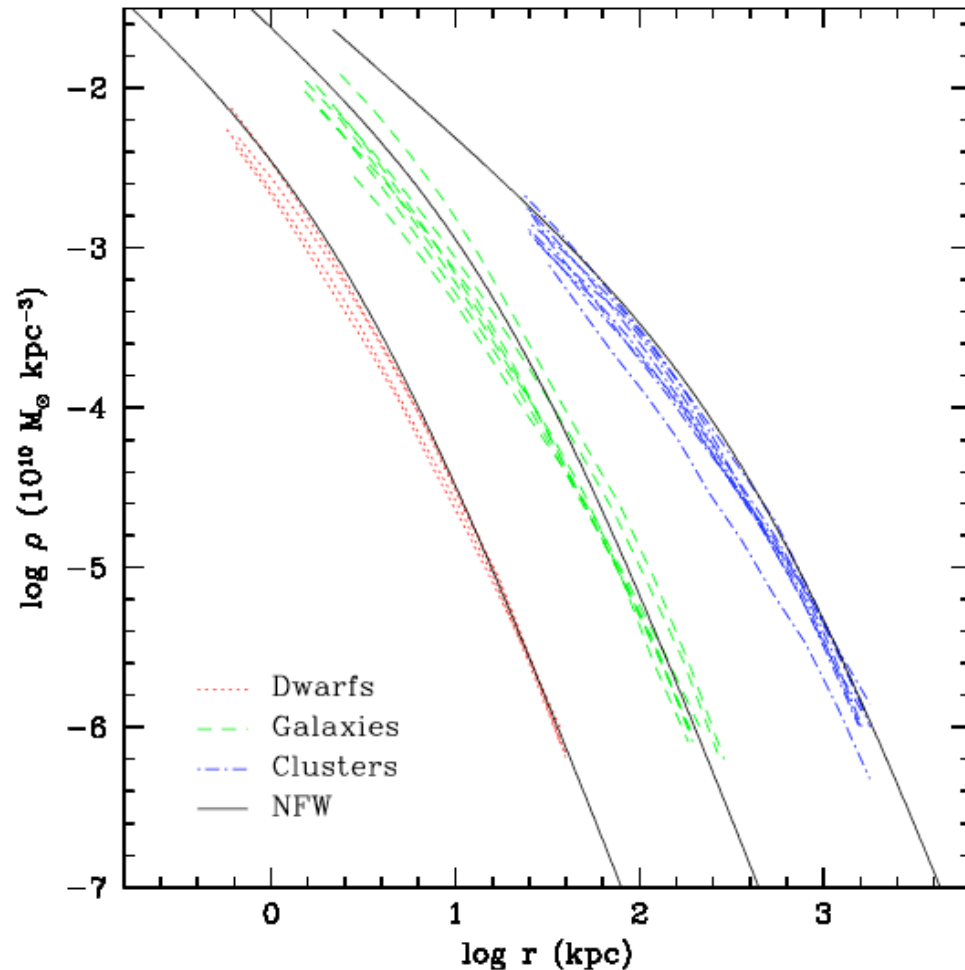
8 Cluster Halos (3.2 Mpc/h box shown)



cl_08 cl_03 cl_05 cl_09 cl_06 cl_02 cl_01 cl_07

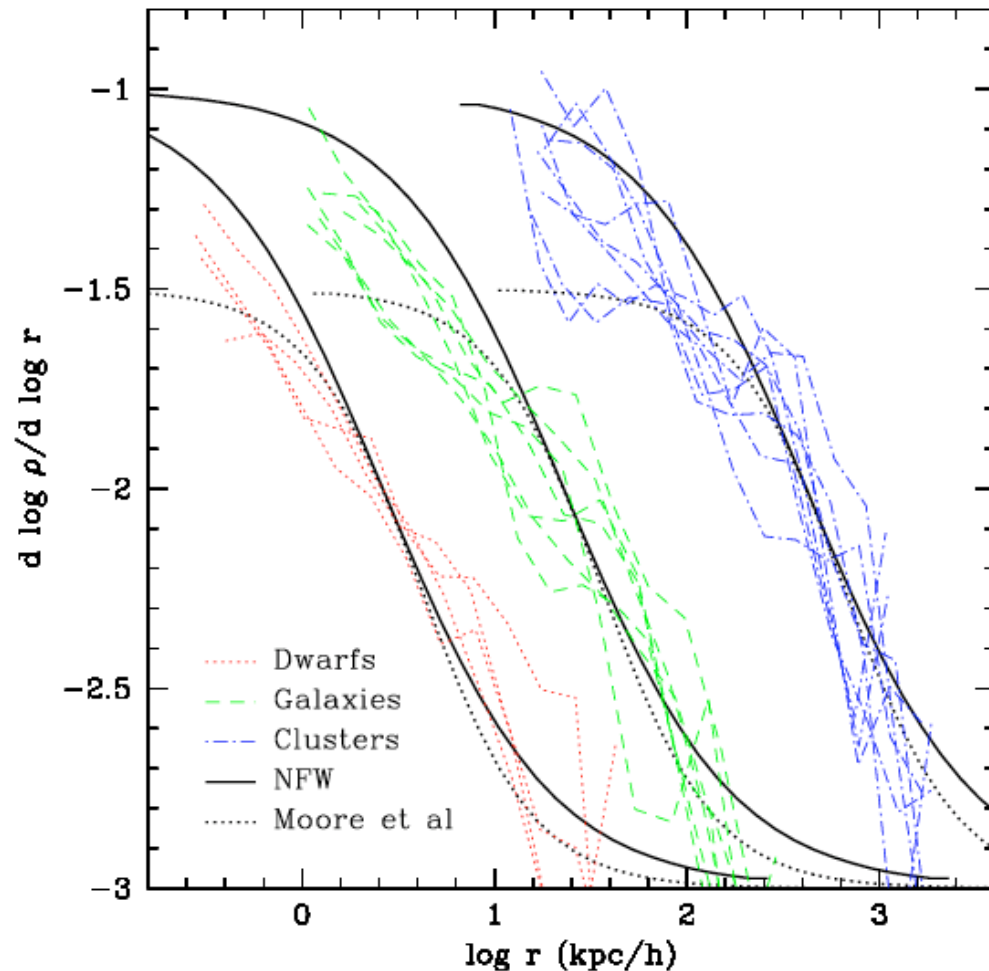
- Halos with 10^6 particles resolved down to 1% of r_{vir}

Universality of Density Profile



- Dark matter density increases toward the centre down to the innermost resolved radius
- Halo density profiles are universal for dwarfs, galaxies and clusters
- Small but significant scatter in shape of density profile from halo to halo

Logarithmic Slope of Density Profile



- Density profiles continue to get shallower all the way down to the innermost resolved radius
- No obvious convergence to an asymptotic value of central slope
- Slope at innermost radius ranges $\beta=1$ to $\beta=1.4$